SNOW CRYSTAL GROWTH AND CONSEQUENT FALL PATTERN

by

Manuel Phillip Langleben, M.Sc.

Being a Thesis Submitted to the Faculty of Graduate Studies and Research of McGill University in Partial Fulfilment of the Requirements for the Degree of Doctor of Philosophy.

August 1953 Montreal, Canada.

ABSTRACT

A theory is developed showing that crystal type is determined by the excess of the ambient vapour density over that at equilibrium with the ice crystal and is verified in an analogue experiment. Changes in crystal habit occur when the vapour density excess is sufficient to overcome the inhibitions to edge and corner growth that must exist if they have higher surface vapour densities than the flat faces of the crystal.

The vapour density field around a crystal growing in water cloud has been solved. Calculations show that cloud can make significant contribution to the rate of growth of ice crystals by diffusion.

Measurements of terminal velocities of snowflakes from motion pictures indicate that velocity is approximately proportional to $(\text{mass})^{0.103}$; the proportionality constant varies with crystal type, degree of riming and of melting.

Analysed radar photographs of snow trails show that the terminal velocity of snowflakes is invariant with height and that aggregation generally occurs in the formation region.

PREFACE AND ACKNOWLEDGEMENTS

This thesis, which is divided into three separate parts, is concerned with a study on snow, its growth habit, its terminal velocity, and the pattern it makes in falling through a wind shear.

Part I deals with the mode of development of the snow crystals and with the factors influencing the type formed. The rate of growth of crystals in supercooled water cloud is also considered. Part II is devoted to a report of measurements made of the terminal velocity of snow aggregates as a function of mass. In Part III, snow patterns in space are analysed from radar photographs and upper air data.

The project reported on was under the supervision of Professor J. S. Marshall, director of the McGill "Stormy Weather" Research Group. It is a pleasure for the author to express sincere gratitude to Dr. Marshall for his stimulating and imaginative direction of the work. Part I of this thesis is the result of collaboration with Dr. Marshall, who specifically contributed to sections 3 and 4. A paper of the same title has been submitted to the Journal of Meteorology under joint authorship.

The author is deeply indebted to Dr. K. L. S. Gunn for assistance in making the observations of Part II, which required more than one person, and for his readiness to enter discussion on the radar work of Part III. Appreciation is acknowledged of Dr. W. Hitschfeld's discerning criticism of the mathematics in Part I. The author is also indebted to Mr. B. A. Power for his upper air analyses and to Messrs. B. A. Stevens and

J. Bordan for operating the radar during the winter 1951-52. Many indirect contributions have doubtless originated in the seminars of the McGill "Stormy Weather" Research Group.

Sincere appreciation is tendered to the Dominion Government who, through its Department of Veterans' Affairs, contributed to the support of the author for six years of his studies; to the U.S.A.F. Geophysics Research Division for financial aid during the last two years; and to the Defence Research Board of Canada who supplied all the equipment and materials needed for the research.

SNOW CRYSTAL GROWTH AND CONSEQUENT FALL PATTERN

Table of Contents

Table of Contents (cont'd)

PART I

A THEORY OF SNOW CRYSTAL HABIT AND GROWTH

1. INTRODUCTION

Nakaya (1951) and his co-workers, and others (aufm Kampe, Weickmann and Kelly, 1951) have shown that type of snow crystal growth depends on the temperature of formation. We have found Nakaya's laboratory investigations most amenable to study and interpretation. In his experiment, ice crystals were formed and grown on a rabbit hair stretched in a stream of cold air which had been moistened just previously by passing it over warm water. At high "supersaturations", dendrites were formed from -13.6 to -17.8C, plates flanked the dendrite range with limits at -9.7 and -20.7C, columns were found still further on the low temperature side and an assortment culminating in needles was present on the other flank.

An ice crystal growing by sublimation in an atmosphere maintained at water equilibrium will assume a temperature which is slightly warmer than that of the ambient air. It is necessary to take this temperature increment into account to obtain the true vapour density excess of water equilibrium over that of the ice crystal. A preliminary investigation of this problem, making use of psychrometric tables, yielded a graph of vapour density excess as a function of temperature at normal atmospheric pressure which was very enlightening. The curve reached its maximum at approximately the temperature favourable for dendritic growth as found by Nakaya (see figure 1.1). The possibility presents itself that crystal type is a function of vapour density excess over ice equilibrium, dendrites requiring maximum values of density excess, plates somewhat less, and so on. Exploration of this possibility calls for a careful derivation of vapour density excess as a function of temperature, and a simple analytical expression has been arrived at.

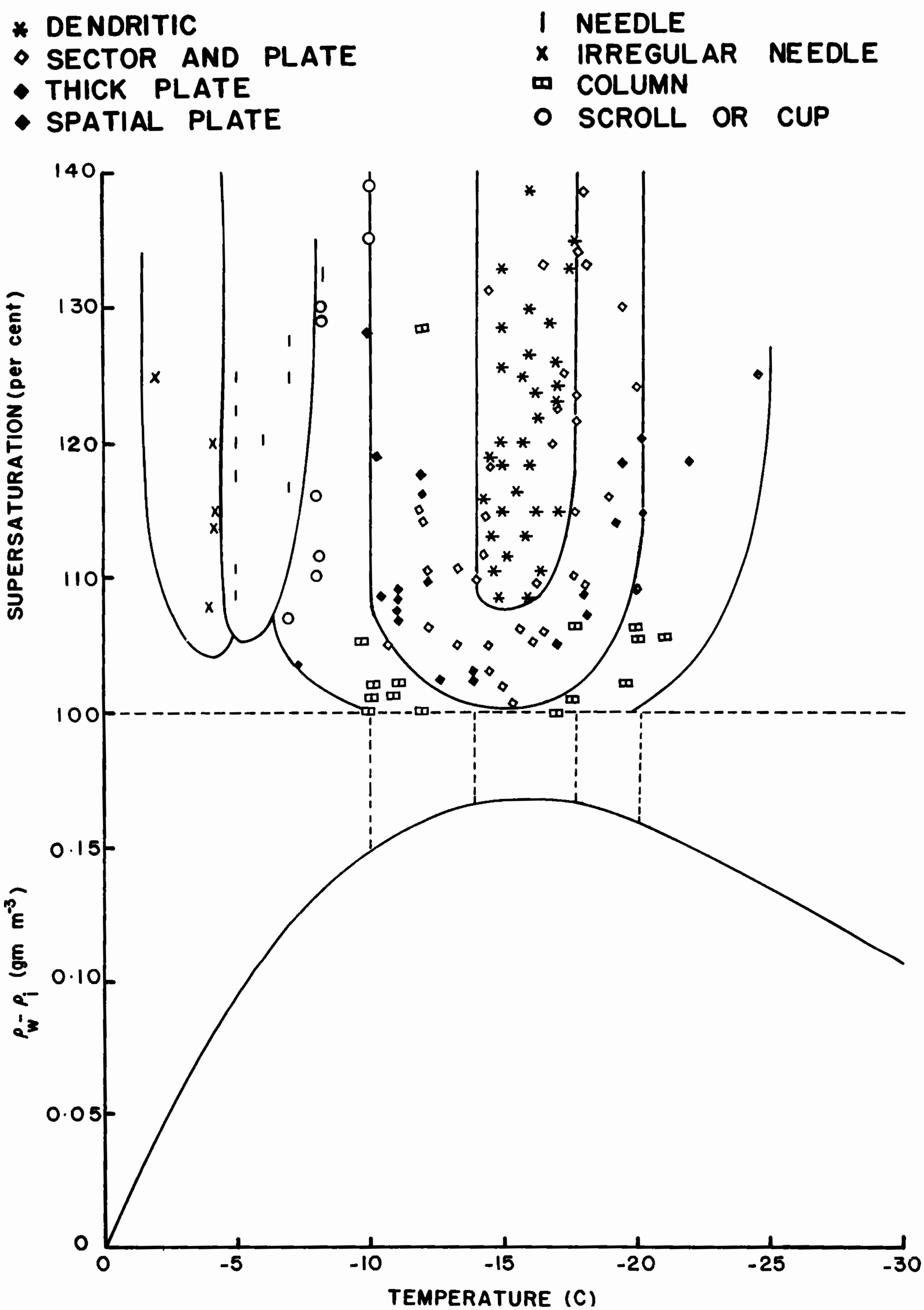

FIG. 1.1 - The top diagram shows the relation between crystal type, "supersaturation" and air temperature as observed by Nakaya's group. The temperature limits for dendrites and plates have been extended down to a curve of vapour density excess against temperature, where the temperature increment by which the growing ice crystal exceeds the air temperature has been taken into account.

Nakaya's "supersaturation" * was surely vapour at water equilibrium (or at some slight supersaturation) plus a cloud of small water droplets; he mentions such droplets. His relative humidities have been converted to density excess over water equilibrium on this basis (figure 1.2). This is a reproduction of the Nakaya diagram, figure 1.1, apart from the conversion mentioned, and the boundary lines are his. The data at high density excess suggest a symmetrical distribution of crystal types about the maximum of the curve of vapour density excess against temperature. Changes in the distribution of crystal type with temperature as the density of supersaturation is reduced imply that this supersaturation density, in either its cloud or vapour component, plays an important role in maintaining the vapour density excess against the inroads of the growing ice crystal. We have found that the small vapour component of the supersaturation density is more significant than any reasonable cloud density can be. The suggestion that vapour density excess of ambient over ice equilibrium is then the basic factor determining the mode of development of the ice crystal is more tenable. The assumption that the equilibrium vapour density at the surface of the crystal varies with its curvature provides a simple mechanism to explain such behaviour. Justification for this has been obtained from an analogue experiment by using a set of electrodes as the crystal model and applying a distant field in the electrolytic solution in which it was immersed.

---

* We have assumed that the "supersaturation" was relative to water equilibrium. There is implicit justification for this in the sequence of Japanese papers (1934-1940). In a recent personal discussion, however, Dr. Nakaya recalled the calculations as being based on ice equilibrium. The representation of crystal type as a function of temperature and "supersaturation" was first presented in a paper in Japanese by Hanajima (1944).

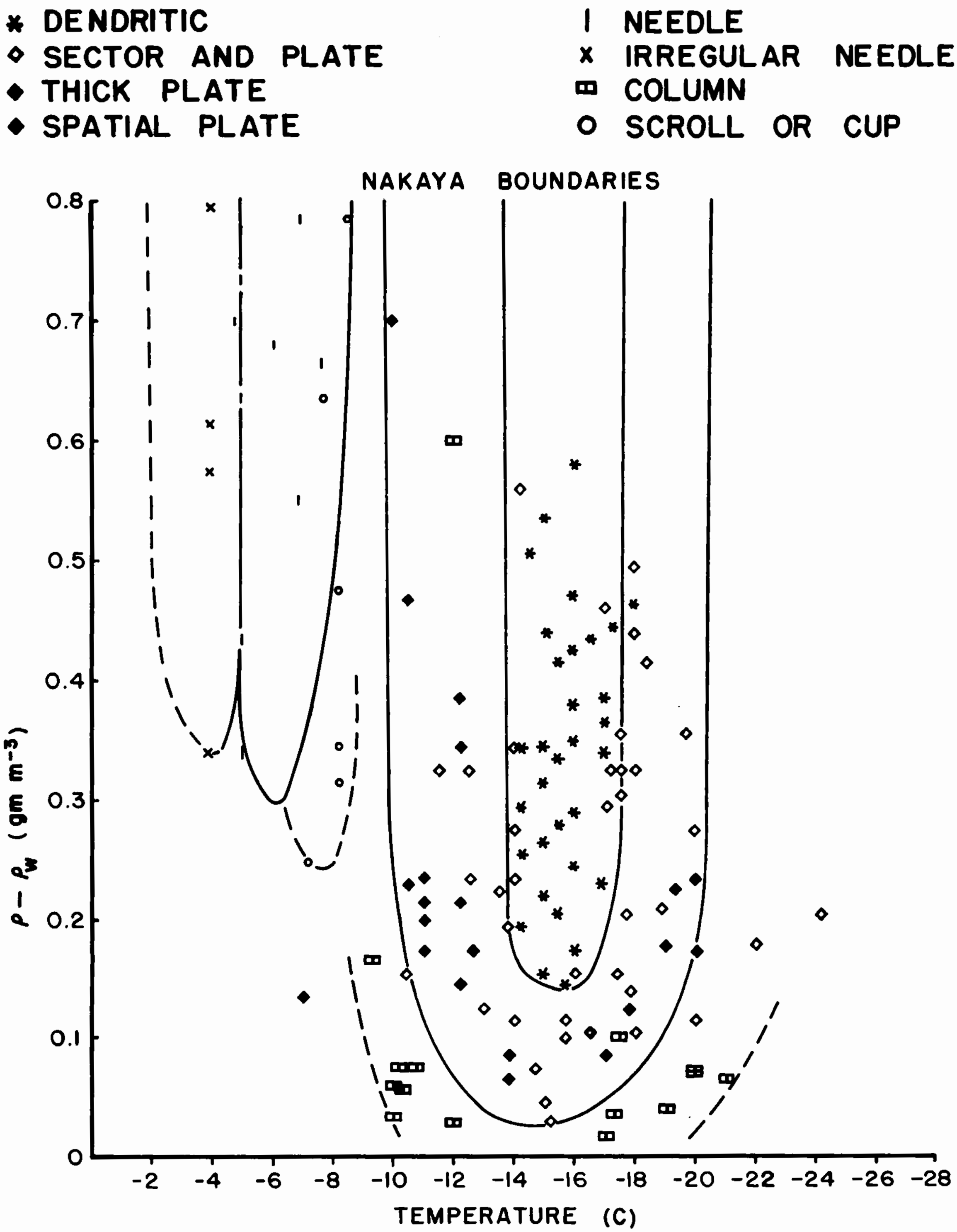

FIG. 1.2 - This is a replot of figure 1.1 with "supersaturation" converted to density excess over water equilibrium. The empirical Nakaya boundaries are also included.

The vapour density excess over ice equilibrium occurs in rate of growth relationships, multiplied by the coefficient of diffusion of water vapour into air. The possibility that rate of growth and so diffusivity are involved in determining the crystal habit has also been explored.

The importance of cloud and its effect on the rate of growth of ice crystals have also been considered. The steady state diffusion equation for an ice particle growing in the presence of cloud has been solved in terms of a parameter involving the sum of the radii of the cloud droplets per unit volume.

2. PSYCHROMETRIC THEORY

2.1 The Psychrometric Equations

Consider an ice crystal which is in an atmosphere supersaturated relative to ice. The ice crystal grows by sublimation (solidification from the vapour phase) and the rate of release of latent heat by this process is proportional to the difference between the ambient vapour density and that at the surface of the crystal (i.e. to the rate of mass transfer). Also the rate of "cooling" of the ice crystal (it actually assumes a temperature above that of the ambient air) by conduction and convection is proportional to the resulting temperature difference between the crystal and its surroundings.

The physical processes outlined are quite similar to those taking place at the bulb of a thermometer which is in a space supersaturated with respect to a thin ice coating on the thermometer bulb. This description essentially fits a wet-bulb thermometer, or more precisely an iced-bulb, at sub-zero temperatures in regions where the relative humidity is greater than 100%. In the light of this similarity, a brief review of psychrometric theory is presented.

The psychrometric tables for a well ventilated wet-and-dry bulb thermometer have been calculated from a semi-empirical equation (Smithsonian Meteorological Tables, 1951) in which the constants were determined experimentally. A comparison will be made with two theoretical equations.

(a) Psychrometric tables. At any given temperature, the psychrometric tables usually list the relative humidities or vapour pressures corresponding to different depressions of the wet-bulb thermometer. No tables have been found, however, to include data above saturation, and some means had to be devised to treat the problem discussed.

A close examination of available tables for sub-zero temperatures showed that the ratio of the difference between ice equilibrium and existing vapour densities to the corresponding depression of the wet-bulb from the dry-bulb temperature was practically independent of temperature and relative humidity. On this basis, it seems justified to extrapolate these results to cases where the ambient vapour densities are greater than those over an ice surface and where the wet-bulb (iced-bulb) would consequently have a "negative depression" (i.e. read higher than the dry-bulb). One can then write an equation to express these findings:

$$\frac{\rho_{aT} - \rho_i(T + \Delta T)}{(T + \Delta T) - T} = \text{const. } f(B) \tag{2.1}$$

where T is the ambient temperature,

$T + \Delta T$ the resulting ice crystal temperature,

ρ_{aT} the ambient vapour density,

$\rho_i(T + \Delta T)$ the vapour density at the surface of the ice crystal, assumed to be at equilibrium with ice at temperature $T + \Delta T$, and

$f(B)$ a function of barometric pressure only.

(b) Diffusion theory. Consider an ice particle, spherical for simplicity and of radius "a", at rest relative to its environment, the ambient vapour density being in excess of that at the surface of the particle.

The rate of mass transfer by diffusion (Maxwell, 1879) to the particle is given by

$$\frac{dm}{dt} = 4\pi aD\ (\rho_{aT} - \rho_i(T + \Delta T)), \tag{2.2}$$

where m is the mass of the ice particle,

t is the time,

and D the diffusivity of water vapour in air.

A similar expression representing the rate of heat transfer by conduction is

$$L\frac{dm}{dt} = 4\pi aK\left[(T + \Delta T) - T\right] \qquad (2.3)$$

where L is the latent heat of sublimation,

and K the coefficient of thermal conductivity of air.

Combining equations (2.2) and (2.3), one obtains for the steady state

$$\frac{\rho_{aT} - \rho_{i(T+\Delta T)}}{(T + \Delta T) - T} = \frac{K}{DL}\,. \qquad (2.4)$$

(c) Convection theory. Assuming that the convective mechanism is of controlling importance (i.e. that the particle is very well ventilated), there results a statement of the Ivory (1822) or August (1825) theory.

Consider a parcel of air of mass m and density d. Let c_p be the specific heat at constant pressure of the air and assume that it does not change appreciably with moisture content. After coming into contact with the ice particle, the parcel gains in sensible heat by an amount $Q = c_p m\left[(T + \Delta T) - T\right]$. The vapour concentration of the parcel decreases, however, from $m\,\rho_{aT}/d$ to $m\,\rho_{i(T+\Delta T)}/d$. The latent heat required to cause this excess to sublimate onto the ice particle is then $Q = Lm(\rho_{aT} - \rho_{i(T+\Delta T)})/d$. The equating of these two heat quantities yields

$$\frac{\rho_{aT} - \rho_{i(T+\Delta T)}}{(T + \Delta T) - T} = \frac{c_p}{L}\,d. \qquad (2.5)$$

2.2 Comparison of the Psychrometric Equations

Assuming a constant barometric pressure, let us first compare the equations as to their dependence on temperature. At sub-zero temperatures both L and c_p are essentially constant. Thus the ratio of vapour density excess to the resulting temperature difference for the convective case (equation 2.5) varies as the air density or inversely with the temperature.

Now the ratio of equation (2.5) to equation (2.4) is

$$\frac{\text{convection}}{\text{diffusion-conduction}} = \frac{dc_p\, D}{K} = \frac{D}{\alpha}$$

where $\alpha = \frac{K}{c_p d}$ is the thermal diffusivity. Montgomery (1947) has listed values of thermal and vapour diffusivities. Using his values, it was found that $D/\alpha = 1.194$ independent of temperature. Thus the diffusion case has the same functional relationship with temperature as does the convection case. The empirical psychrometric equation, however, shows no apparent dependence on temperature. These results are summarized in table 1 for an atmospheric pressure of 1000 mb. The values at any other pressure may be obtained by multiplying those listed by the ratio of the existing pressure to standard pressure.

Table 1

$\frac{\Delta\rho}{\Delta T}$ ($gm\ m^{-3} deg\ C^{-1}$)	T(C)	-2	-10	-20	-30
Psychrometric tables		0.539	0.539	0.539	--
Diffusion		0.379	0.393	0.408	0.425
Convection		0.452	0.469	0.487	0.527

Since the physical mechanisms, those of heat and vapour transfer, are the same in the three cases discussed, some explanation is necessary to account for the discrepancies displayed in table 1. The convection equation results if it is assumed that the transfer rates for heat and vapour are alike when expressed in the dimensions "per unit area per unit time". The diffusion-conduction equation differs from the former by the ratio α/D, the ratio of thermal to vapour diffusivities. In this case the rates of material and heat transfers are different and so the diffusivities are introduced. The fact that the empirical psychrometric equation does not depend on temperature in the same way and is in further numerical disagreement as well may be due to stem corrections for heat losses which have been included automatically in the psychrometric tables (Ferrel, 1886).

In all subsequent use of these equations, equation (2.4) will be emphasized. For the early stages of crystal development, it may be assumed that the crystal is almost at rest relative to the surrounding air and that therefore the diffusivities are the controlling quantities.

2.3 Derivation of $\Delta\rho$ vs T Curves

It has been shown how to obtain the ratio of the vapour density excess (henceforth called $\Delta\rho$) to the temperature difference by means of the psychrometric equations. One is, however, more interested in determining $\Delta\rho$ as a function of temperature and to a good degree of accuracy. Houghton (1950) and Wexler and Boucher (1952) have computed values of $D\,\Delta\rho$ which occurs in rate of growth relationships. Their calculations employed the laborious process of trial and error. We have derived an analytical expression, given below, for the vapour density excess which eliminates the tedium of their calculations. Recently Mason (1953) has presented a graph essentially the same as Houghton's. The theory on which his computations are based involves several approximations which appear quite reasonable. However, his integration of the Clausius-Clapeyron equation for equilibrium vapour pressures of ice, using the perfect gas law as equation of state, does not seem entirely justified when the painstaking efforts of Washburn (1924) and Goff and Gratch (1946) are considered.

A quick graphical method to determine $\Delta\rho$ may be used in conjunction with the results of section 2.2. This method, resulting in a value of $\Delta\rho$, is illustrated in figure 2.1, where ambient has been taken as water equilibrium. Thus, given the ambient temperature T and vapour density ρ_a, a straight line of slope K/DL (using the diffusion-conduction equation) through the point ρ_a, T will intersect the ρ_i against T curve at $\rho_i(T + \Delta T)$ and $T + \Delta T$.

Alternatively, for greater accuracy, one may calculate $\Delta\rho$ analytically and using tabulated values of equilibrium vapour pressures over water and over ice. For this purpose the tables and formulae of Washburn, giving equilibrium vapour pressures as a function of temperature, were used. Now Δp, the difference between the ambient vapour pressure and that at the crystal surface, can be represented as

$$\Delta p = \Delta p\,]_T + \frac{dp_i}{dT}\,\Delta T \qquad (2.6)$$

where $\Delta p\,]_T$ is the pressure difference at constant temperature T,

p_i the saturation vapour pressure over ice at temperature T,

and $\frac{dp_i}{dT}$ its variation with temperature, at temperature T, as obtained by using finite differences.

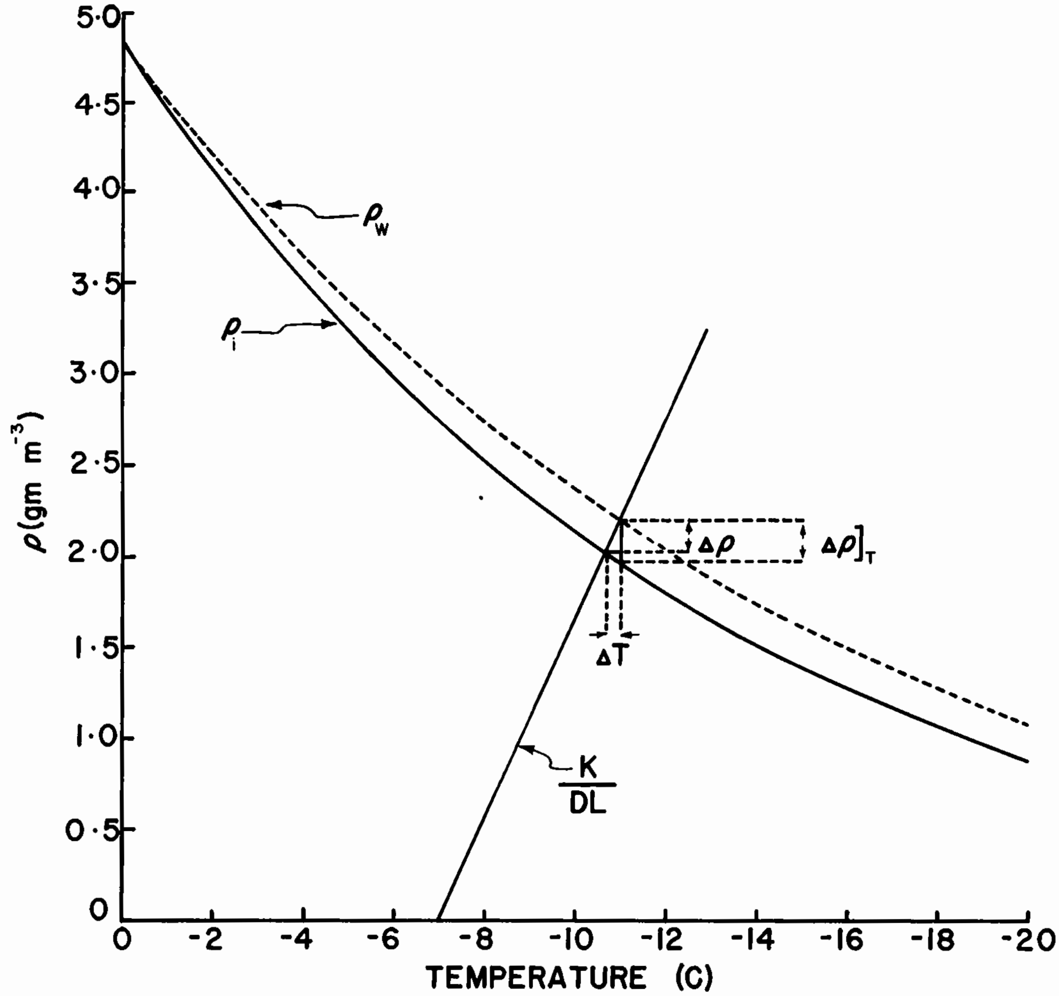

FIG. 2.1(a) - The temperature of an ice crystal surrounded by vapour of density ρ_w and temperature T is T + ΔT. The vapour density excess is therefore $\Delta\rho = \rho_{wT} - \rho_{i(T + \Delta T)}$. A line of slope K/DL through the point ρ_w,T intersects the ρ_i curve to give T + ΔT and $\rho_{i(T + \Delta T)}$.

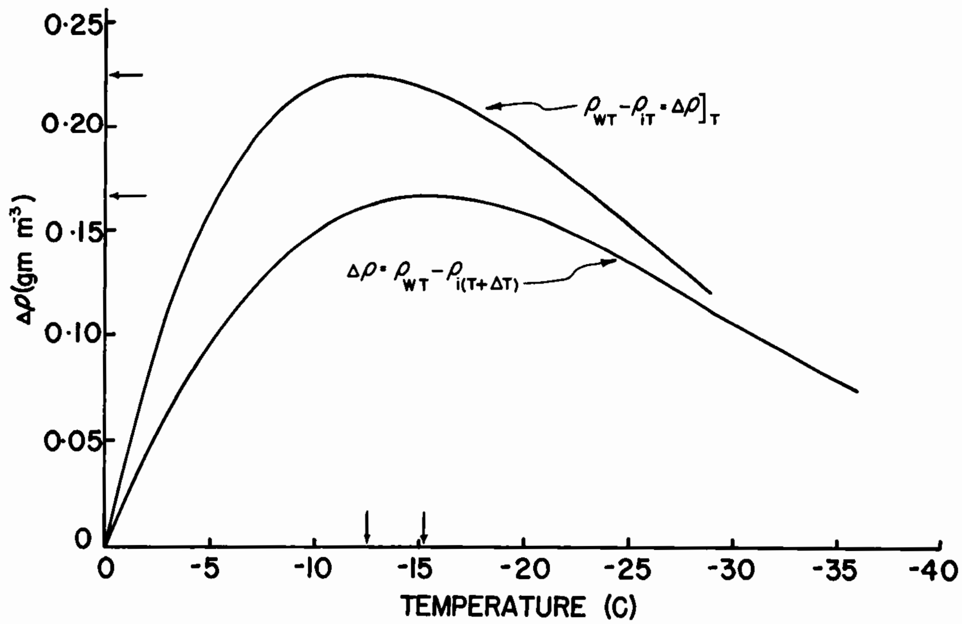

FIG. 2.1(b) - The water equilibrium vapour density exceeds the ice equilibrium at the ice temperature by a maximum of 0.1676 gm m^{-3} at -15.4 C. For comparison, if the ice were at the same temperature as the vapour, the excess would reach a maximum of 0.224 gm m^{-3} at -12.5 C.

Since $\Delta\rho/\Delta T = -K/DL$ according to equation (2.4), the minus sign having entered if the temperature interval is taken in the same sense as in equation (2.6), the above becomes

$$\Delta p = \Delta p\,]_T - \frac{dp_i}{dT}\;\Delta\rho \Big/ \frac{K}{DL}\;. \tag{2.7}$$

Substituting for Δp by differentiating the gas equation, we have that

$$\frac{R}{M}\,T\Delta\rho\; - \frac{p_i}{T}\,\Delta\rho \Big/ \frac{K}{DL} = \Delta p\,]_T - \frac{dp_i}{dT}\,\Delta\rho \Big/ \frac{K}{DL}$$

where M is the molecular weight of water vapour,

and R the universal gas constant.

Thus

$$\Delta\rho = \frac{\Delta p\,]_T}{\frac{RT}{M} + \left[\frac{dp_i}{dT} - \frac{p_i}{T}\right] \Big/ \frac{K}{DL}}\;. \tag{2.8}$$

If convection is thought to be the influencing mechanism the only change in equation (2.8) is the replacement of K/DL by $c_p d/L$. A corresponding change is needed if the empirical psychrometric equation is used.

Calculations of $\Delta\rho$ were made at both 1000 and 500 mb. The results are represented graphically in figure 2.2 where the ambient conditions were assumed to be those at equilibrium with respect to water. It is worth noting that although the $\Delta\rho/\Delta T$ values listed in table 1 differ by more than 25% at -15C, the corresponding values of $\Delta\rho$ differ by only 5%. Thus the discrepancies between the theories outlined in section 2.1, which appeared very serious, have a much lesser effect on the $\Delta\rho$ curves than might be expected. At 1000 mb, the curves of figure 2.2 peak at -14.8, -15.1, and -15.4C on the bases of the three psychrometric equations, and the values of $(\Delta\rho)_{max}$ decrease slightly as shown. At 500 mb the same sort of temperature

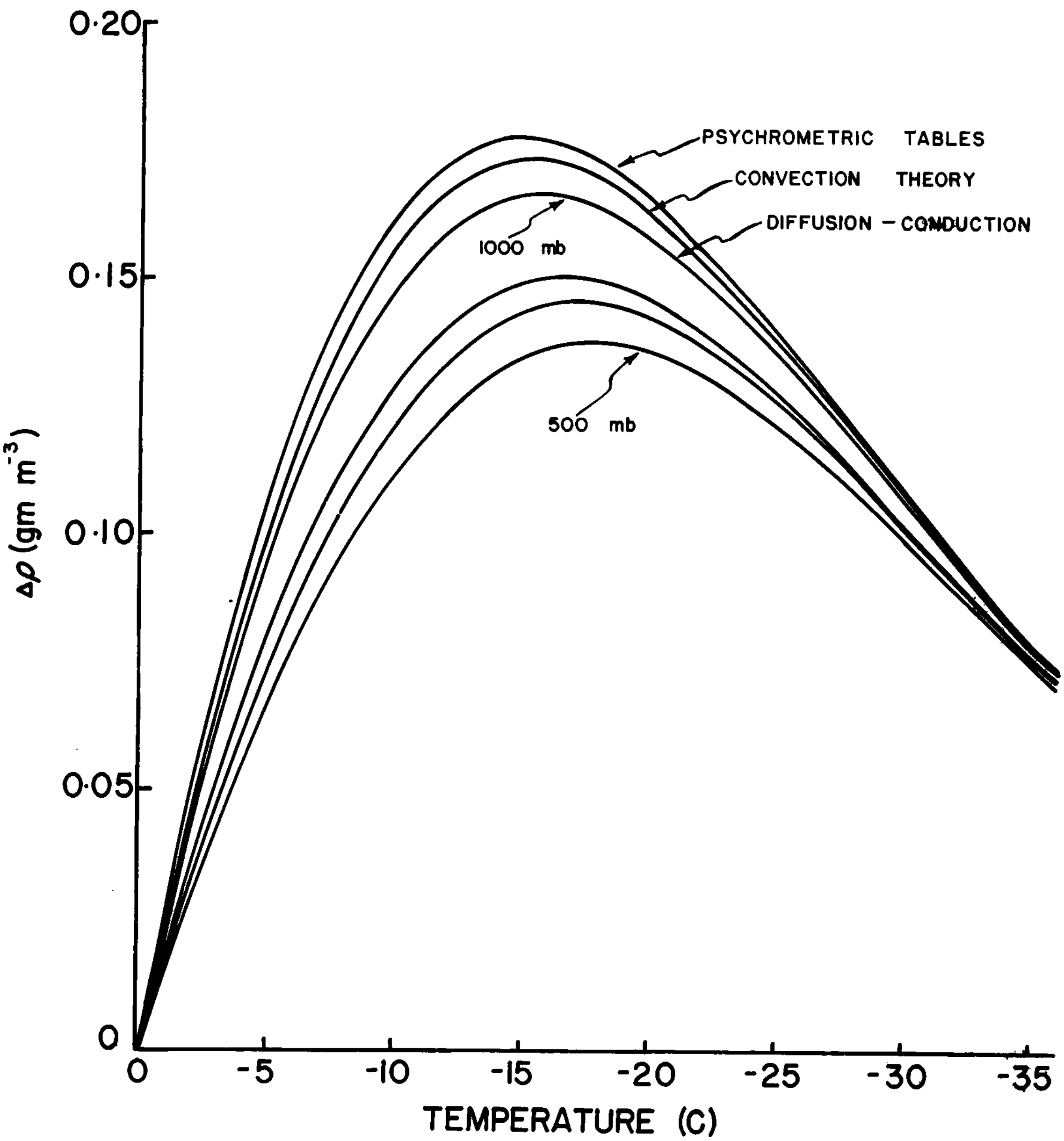

FIG. 2.2 - This shows the dependence of the excess of the water equilibrium vapour density over that of the growing ice particle on barometric pressure and on the theory used. At 1000 mb the curves peak at -14.8, -15.1 and -15.4C and $(\Delta\rho)_{max}$ decreases as shown.

shift is experienced, all curves moving as well about one degree towards lower temperatures. Furthermore, although it was seen that the $\Delta\rho/\Delta T$ values were directly proportional to the barometric pressure, the $\Delta\rho$ curves are a much less sensitive function of this pressure. For instance, the ratio $(\Delta\rho)_{1000\ mb}/(\Delta\rho)_{500\ mb}$ at -15C is only about 1.2.

3. TYPE OF GROWTH AS A FUNCTION OF VAPOUR DENSITY EXCESS

3.1 Introduction

The laboratory experiments of Nakaya indicate that the mode of crystal development is dependent on temperature. Now the temperature range for a given type of growth, according to the adjusted Nakaya diagram (figure 1.2), increases rapidly at first with $(\rho - \rho_w)$, where ρ is the total density in the form of vapour and cloud, and ρ_w the equilibrium vapour density over water. The boundaries first attain their maximum width or temperature limits at about $(\rho - \rho_w) = 0.3$ gm m^{-3}.

His investigations were presumably carried out at normal atmospheric pressures and, extending these temperature limits to a curve of $\Delta\rho = (\rho_w - \rho_i)$ at 1000 mb, it is seen that they intersect almost equal values of $\Delta\rho$ for the plate and dendrite regions (figure 1.1).

3.2 The Nakaya "Supersaturation"

Nakaya obtained what he called supersaturation by mixing cold saturated air with warm saturated air. A supersaturated mixture resulted and a cloud of fine droplets was formed as is mentioned specifically in his Compendium article.

Now the total density ρ of the mixture exists wholly in the vapour phase immediately after mixing so that at time $t = 0$, $\rho = \rho_v$ and $\rho_c = 0$, where ρ_v and ρ_c are the densities in the vapour phase and in the form of cloud respectively. Also at all time t, the total density is the sum of the cloud density and the vapour density, i.e. $\rho = \rho_v + \rho_c$.

Assume that a certain number n of cloud droplets is formed per unit volume. The rate of increase of cloud density with time at time t will be proportional to the instantaneous value of the vapour density excess $(\rho_v - \rho_w)$ multiplied by nr_c where r_c is the radius of the cloud droplets, assumed to be of equal size. In fact,

$$\frac{d\rho_c}{dt} = 4\pi D\, nr_c(\rho_v - \rho_w).$$

But the cloud density

$$\rho_c = \frac{4}{3}\pi\sigma\, nr_c^3,$$

where σ is the density of water. So that

$$\frac{d\rho_c}{dt} = A\rho_c^{1/3}(\rho_v - \rho_w)$$

in which $A = 4\pi\, Dn(3/4\pi\sigma n)^{1/3}$ has the units $gm^{-1/3}$ cm sec^{-1} when the volume under consideration is 1 m^3. Now

$$\rho_c = \rho - \rho_v \qquad \text{and} \qquad \frac{d\rho_c}{dt} = -\frac{d\rho_v}{dt}.$$

Therefore

$$-\frac{d\rho_v}{dt} = A\left[(\rho - \rho_w) - (\rho_v - \rho_w)\right]^{1/3}(\rho_v - \rho_w). \quad (3.1)$$

Equation (3.1) cannot be solved exactly for ρ_v as a function of time, but an approximate solution may be obtained by the following procedure. Figure 3.1a is a plot of $(\rho_v - \rho_w)/(\rho - \rho_w)$ against $-\frac{d\rho_v}{dt}/A(\rho - \rho_w)^{4/3}$. By choosing fine intervals of the ordinate and multiplying by the abscissa, the curve of figure 3.1b results, where $(\rho_v - \rho_w)/(\rho - \rho_w)$ is plotted as before and $At(\rho - \rho_w)^{1/3}$ is the abscissa. This is a measure of the decay of $(\rho_v - \rho_w)$ or supersaturation with time. The corresponding increase of cloud density ρ_c is given by the inverse of this curve.

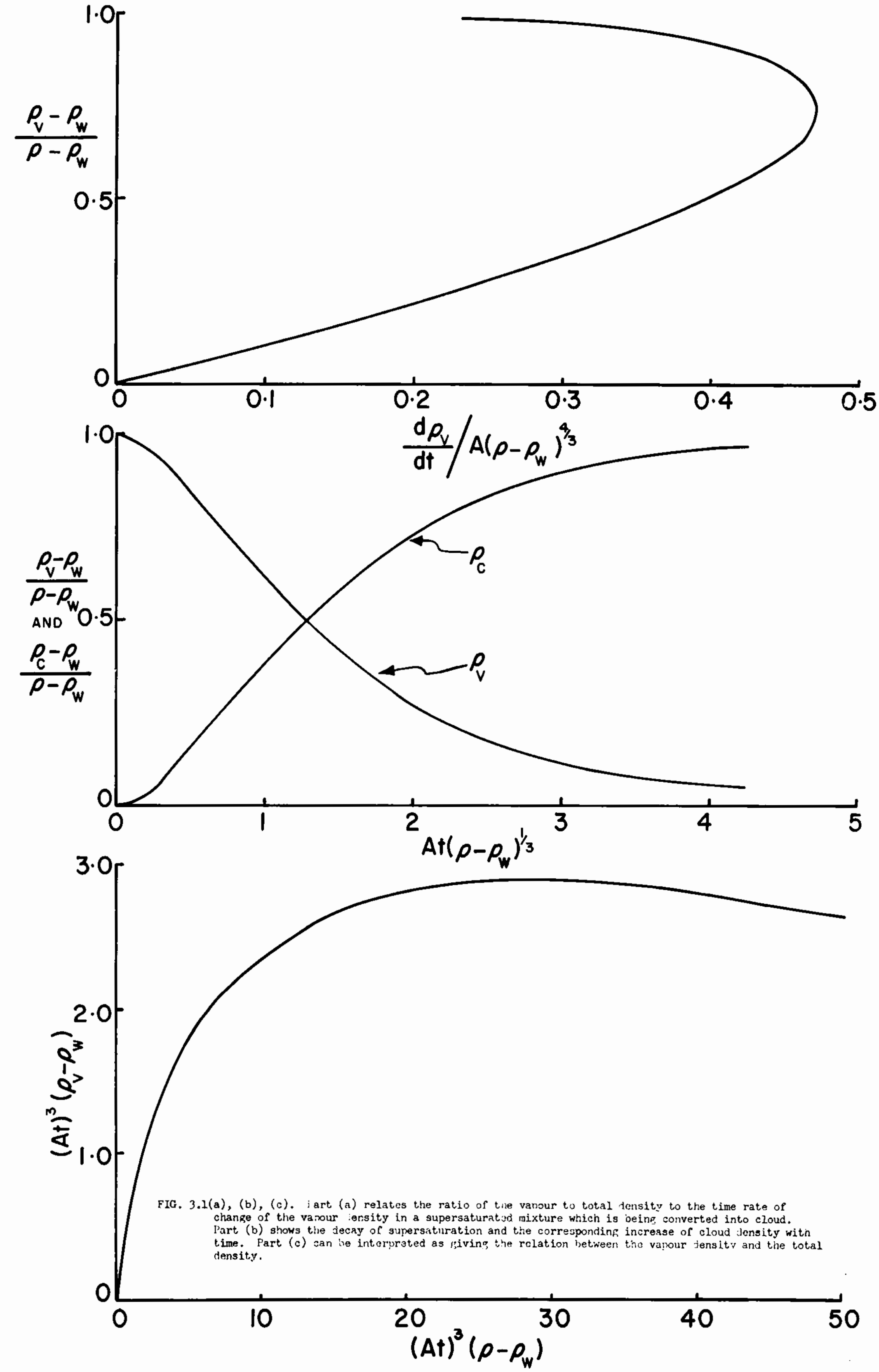

FIG. 3.1(a), (b), (c). Part (a) relates the ratio of the vapour to total density to the time rate of change of the vapour density in a supersaturated mixture which is being converted into cloud. Part (b) shows the decay of supersaturation and the corresponding increase of cloud density with time. Part (c) can be interpreted as giving the relation between the vapour density and the total density.

Figure 3.1c is a graph of $(\rho_v - \rho_w)(At)^3$ versus $(\rho - \rho_w)(At)^3$ and is obtained from figure 3.1b. It is seen that for a given $(At)^3$, $(\rho_v - \rho_w)$ increases rapidly with $(\rho - \rho_w)$, reaches a maximum and then decreases very slowly. (It is felt that this slight decrease is perhaps not real, but rather due to the graphical solution necessarily employed in going from a to b in figure 3.1.) This indicates that the degree of supersaturation possible attains a maximum for some value of $(\rho - \rho_w)$ and that for greater values of total density, greater supersaturations cannot be achieved.

3.3 Loci of Constant $(\rho_v - \rho_i)$

From figure 3.1c, it is seen that $(\rho_v - \rho_w)(At)^3$ has its maximum value at $(\rho - \rho_w)(At)^3 = 30$. Now the boundary lines for dendrites and plates on the Nakaya diagram (figure 1.2) appear to attain their widest temperature limits at a value of $(\rho - \rho_w) = 0.3$ gm m^{-3}. This would indicate that the appropriate $(At)^3$ for his mechanism of convective mixing and flow be set equal to $30/(0.3 \text{ gm m}^{-3}) = 100$ gm^{-1} m^3. Accepting this value of $(At)^3$, it is possible to convert $(\rho - \rho_w)$ to $(\rho_v - \rho_w)$ and vice-versa by means of figure 3.1c.

Loci of constant $(\rho_v - \rho_i)$, where ρ_i is the equilibrium vapour density over the ice crystal surface, can be superimposed on the Nakaya data using the equation

$$(\rho_v - \rho_w) = (\rho_v - \rho_i) - (\rho_w - \rho_i)$$

$$= \text{constant} - (\rho_w - \rho_i) \text{ along a given locus.}$$

A set of such loci is shown in figure 3.2, which includes also scales of both $(\rho - \rho_w)$ and $(\rho_v - \rho_w)$. The locus $(\rho_v - \rho_i) = 0$ is our previous

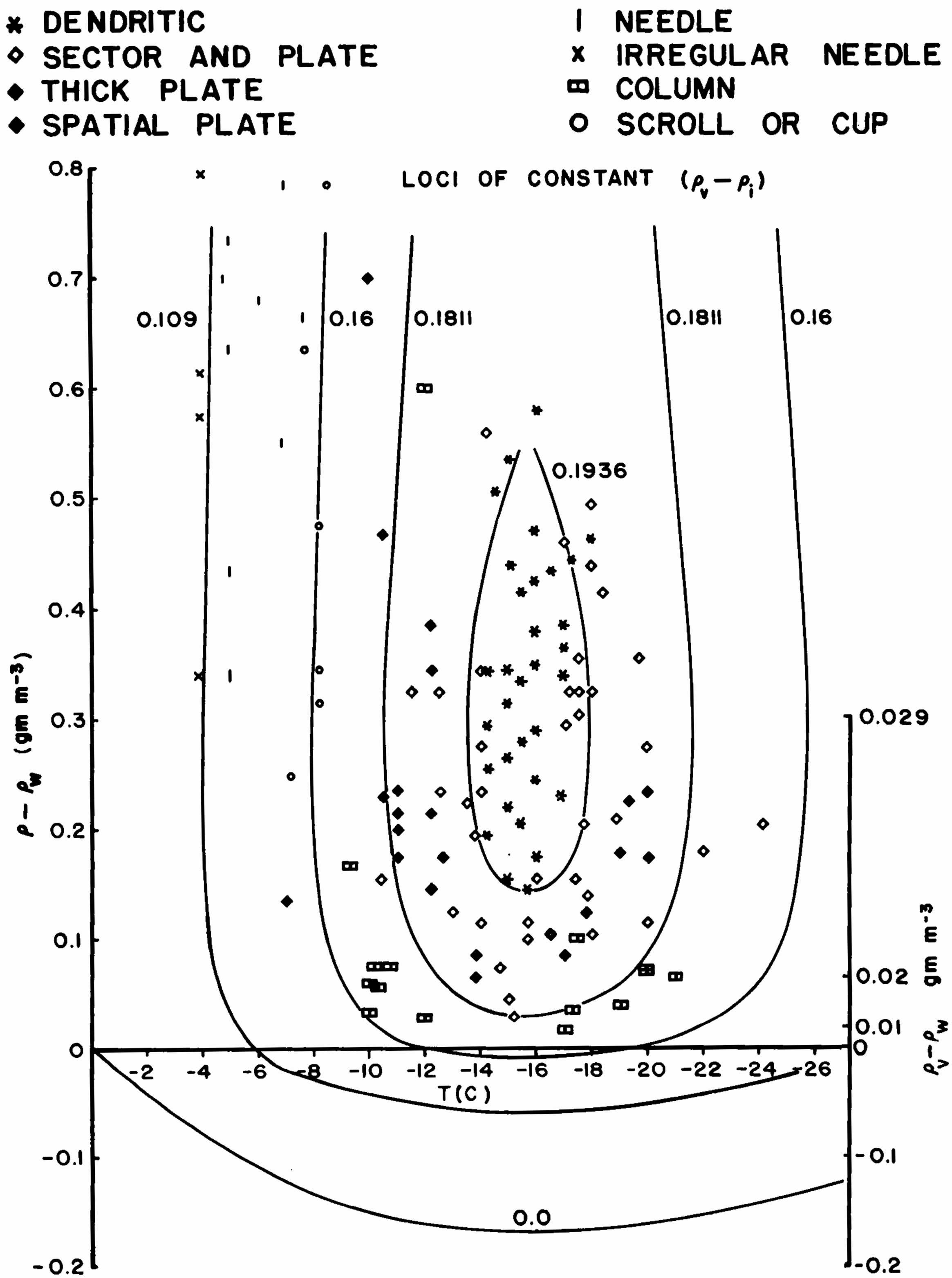

FIG. 3.2 - Loci of constant excess of ambient vapour density over that existing at the ice particle are superimposed on the Nakaya data. These serve to define the crystal type domains as effectively as his empirical ones. A measure of the true supersaturation is shown by the scale on the right (a scale of the excess of the vapour density over water equilibrium) which increases to a maximum of 0.03 gm m^{-3} when the total density above water equilibrium is 0.3 gm m^{-3}.

curve (figure 2.2) of $\Delta\rho = (\rho_w - \rho_i)$ which has been inverted. Loci of constant $(\rho_v - \rho_i)$ have also been included to bound the regions favourable for the formation of dendrites, plates, columns and needles. These boundaries fit the Nakaya data as well as his empirical lines which are shown in figure 1.2. In fact, the locus $(\rho_v - \rho_i) = 0.1811$ gm m^{-3} appears to enclose the plate region even better than does Nakaya's corresponding boundary.

The mechanism discussed calls for but a very slight supersaturation since the maximum value of $(\rho_v - \rho_w)$ is about 0.03 gm m^{-3}. The maximum degree of supersaturation needed is given in table 2. The lack of crystals in the upper right of the Nakaya diagram may be explained, since supersaturations approaching 105% would be difficult to achieve experimentally and would have to be maintained for the order of 6 hours.

It is interesting to point out that according to Howell (1949) supersaturations of the order of 2% can arise in the atmosphere by the natural uplift in frontal systems.

Table 2

T	ρ_w	Max. relative humidity (relative to water)
C	gm m^{-3}	%
0	4.847	100.5
-5	3.407	100.8
-10	2.358	101.2
-15	1.605	101.8
-20	1.074	102.7
-25	0.7047	104

3.4 Upper Air Data

Gold and Power (1952, 1953) estimated the formation level of snow in the atmosphere from an analysis of upper air data and correlated the temperature and pressure at the formation level with the crystal type (or types) reaching the surface. Their results are plotted in figure 3.3 as crystal type as a function of temperature and barometric pressure.

If vapour density excess over ice equilibrium is to be the controlling mechanism for the mode of crystal formation, then it should not be possible for dendrites to form and grow at a pressure of say 500 mb because of the decrease of effective vapour density excess with decreasing pressure (figure 3.4). This is quite contrary to experience.

On the other hand, if type of growth is intimately related to rate of growth ($D\Delta\rho$), dendrites which are limited to a 4 deg C interval at 1000 mb should flourish over a temperature range of about 30 deg C at 500 mb (figure 3.5). The latter is most unlikely and the data of Gold and Power show no such increase in spread with decreasing pressure for dendrites (or for any other crystal type). Also the Nakaya temperature limits do not straddle the $D\Delta\rho$ curve at 1000 mb as symmetrically as they do the $\Delta\rho$ curve.

In the case of the Nakaya laboratory experiment, the crystal habit or mode of development has been shown to be a function of vapour density excess. It is clear, however, that some additional factor must be introduced to explain crystal formation in the natural atmosphere, for with decreasing air pressure the psychrometric values change and the vapour density excess decreases.

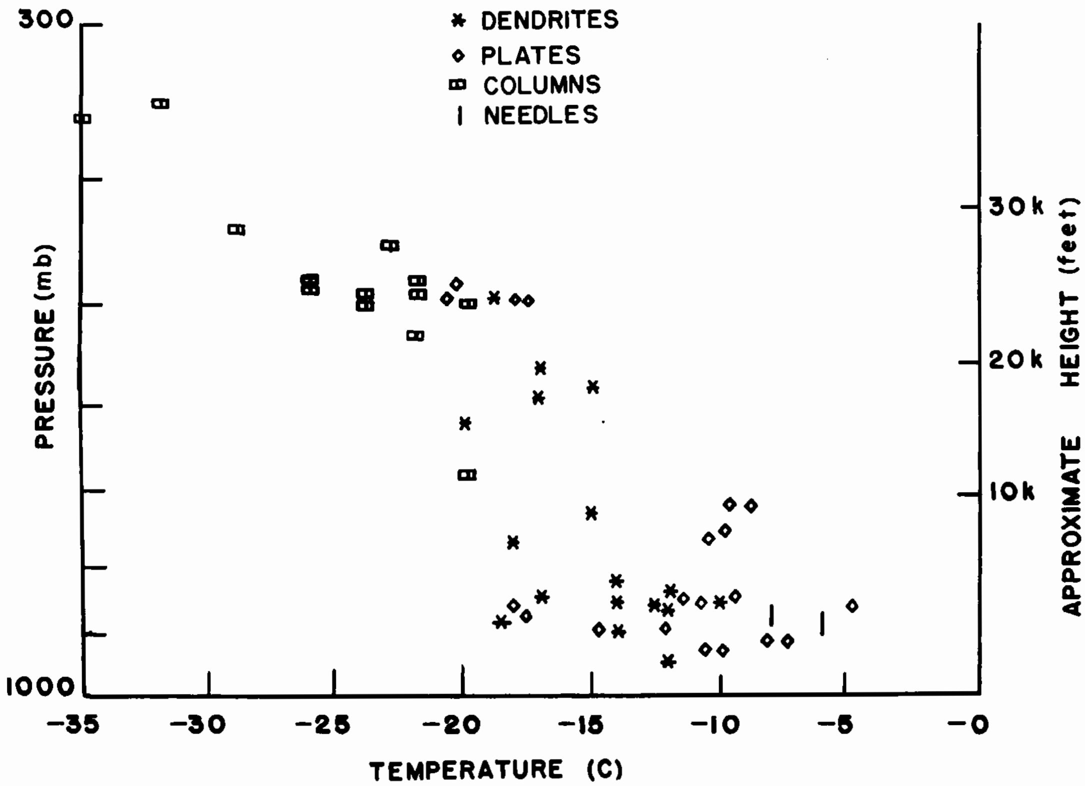

FIG. 3.3 - Crystal type is plotted against pressure and temperature from the observations of Gold and Power and shows a drift towards lower temperatures as the pressure decreases. The scale at right gives the estimated height of formation of the snow.

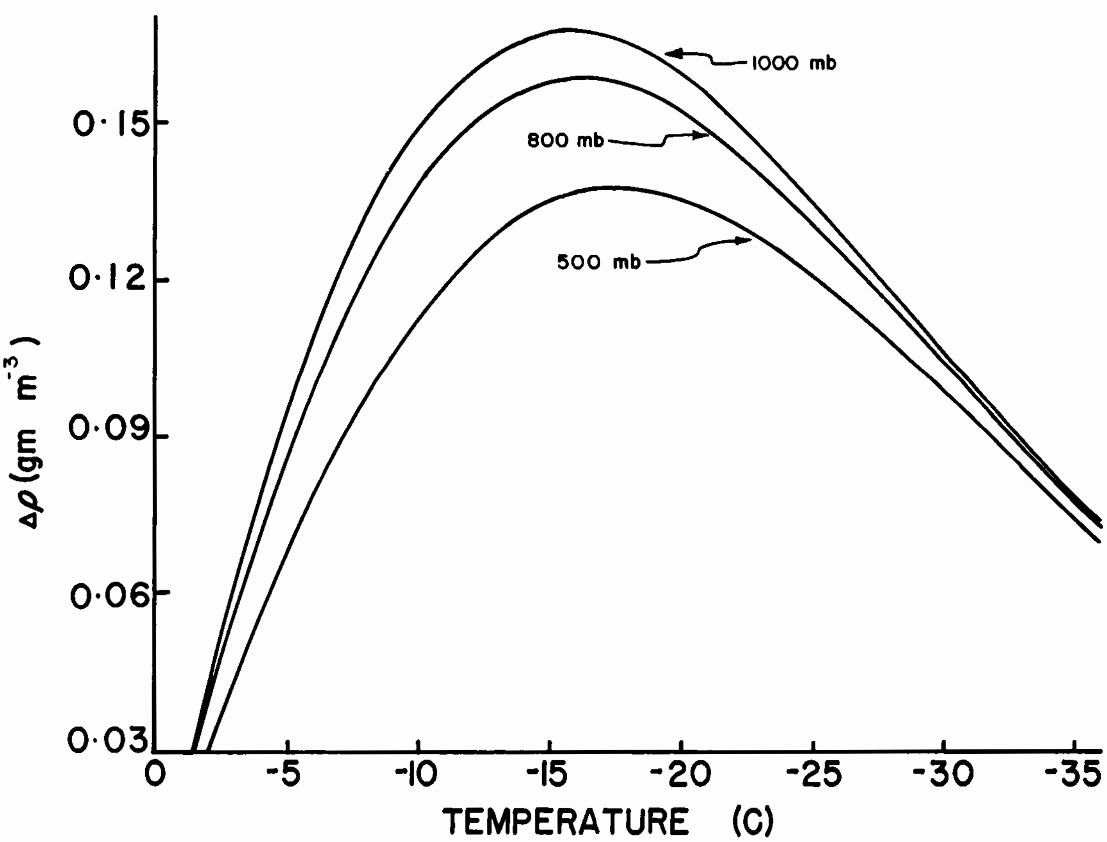

FIG. 3.4 - The decrease of the vapour density excess with decreasing pressure would make it impossible to achieve dendritic growth at higher altitudes.

3.5 Adjusting for Pressure Dependence

Let us assume that crystal type is a function of vapour density excess multiplied by some power n of the ratio of normal to prevalent air pressure B_o/B. By choosing $n = 0.286$* (it could possibly be somewhat greater) and multiplying the $\Delta\rho$ curves of figure 3.4 by $(B_o/B)^n$, the results obtained are as given in figure 3.6. The curves are now of the same general shape and peak at equal values of the ordinate.

Dendrites, which require a certain value of vapour density excess at 1000 mb, can now grow at lower pressures as well, the temperature range shifting slightly towards lower temperatures (and similarly for other crystal types). This is in good agreement with the findings of Gold and Power (figure 3.3) who observed a shift towards lower temperatures as the atmospheric pressure decreased.

---

* Although the power $n = 0.286$ was first chosen arbitrarily to bring the peaks of the $\Delta\rho$ curves to the same value at all pressures, it may be that there is some physical justification for this. The potential temperature which defines an adiabatic process involves $(B_o/B)^{R/c_p} = (B_o/B)^{1-1/\gamma}$, where γ is the ratio of specific heats of air (Handbook of Meteorology, 1945). On substituting the appropriate values for air, $R/c_p = 1 - 1/\gamma = 0.286$.

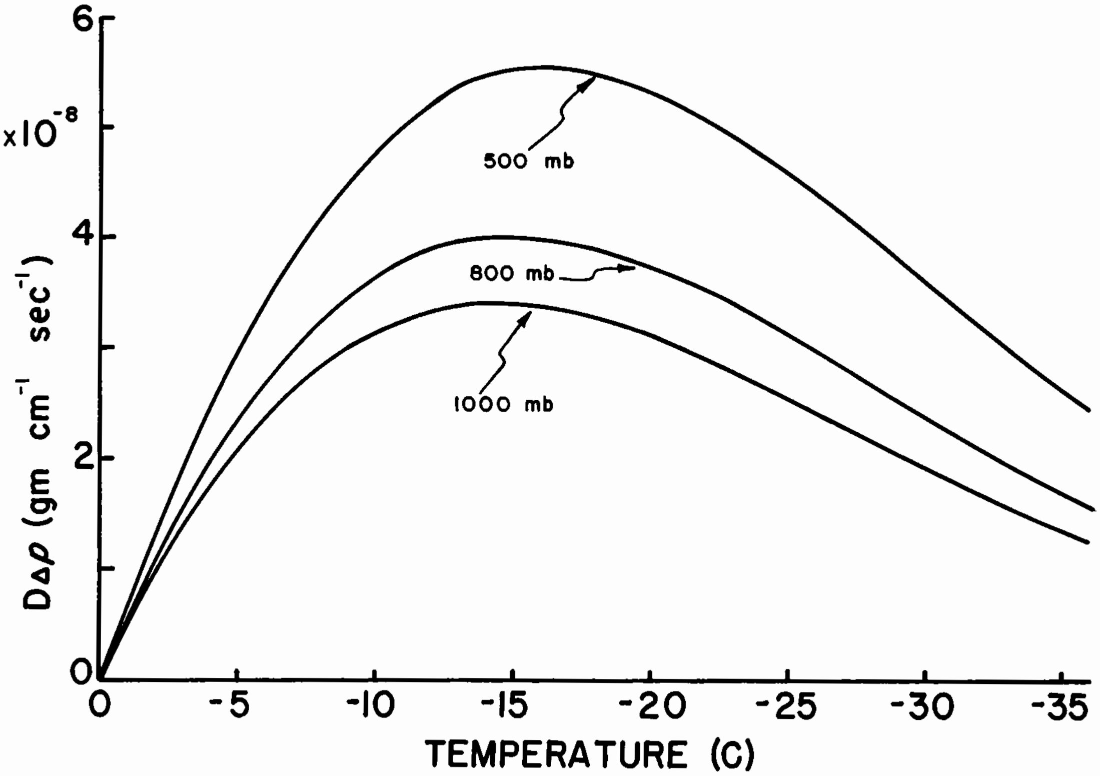

FIG. 3.5 - If crystal type is related to rate of growth, i.e. $D\Delta\rho$, it should be possible for dendrites to form over a very wide temperature range in the atmosphere, since $D\Delta\rho$ increases with decreasing pressure as shown here.

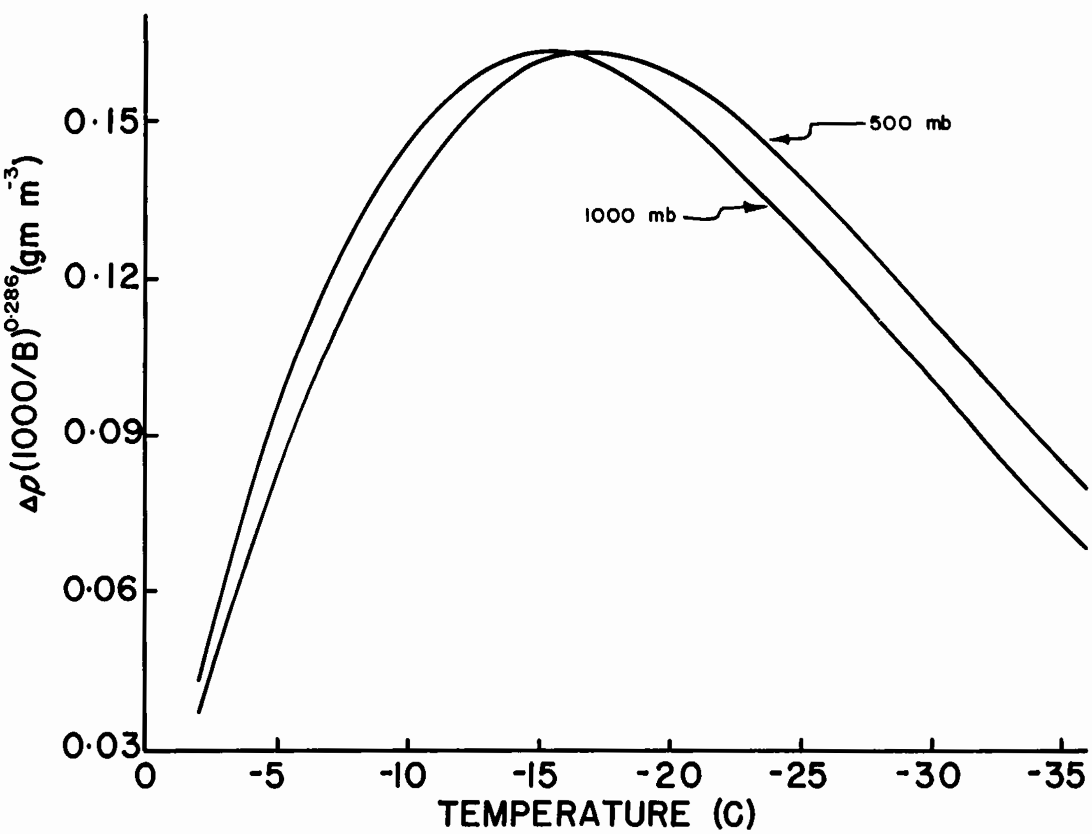

FIG. 3.6 - Adjusting the $\Delta\rho$ curves as shown causes the curves to peak at equal values. The shift towards lower temperatures with decreasing pressure fits the observations of Gold and Power.

4. A POSSIBLE TRANSITION MECHANISM

4.1 Surface Vapour Density

Thus far the assumption has been made that the vapour density existing at the surface of the ice crystal was at equilibrium with respect to a flat ice surface at the temperature of the crystal. This is in fact not the case, for surface vapour density is a function of curvature as has been well established for tiny water droplets. Taking the hexagonal plate as an example, the surface vapour density over the edges must be greater than over its flat surfaces and greater still at the corners where the curvature is highest.

The idea has been roughly verified by Nakaya (1938) who placed snow crystals in a stoppered bottle whose inside walls were coated with hoar frost, the vapour density in the bottle being then more or less at equilibrium to a flat ice surface. He observed that the crystal did not sublime and disappear, but transformed itself into a shapeless pellet after some time. Since the walls of the bottle were covered with ice, there could be but slight net transfer of mass from the crystal to the walls. But because of the effect of curvature on surface vapour density, a mass transfer occurred from the sharper edges of the crystal to those less curved until it finally resembled an ice pellet.

As will be seen, the vapour density field, which is radially symmetric for a sphere, increasing proportionally with reciprocal distance, becomes distorted in the near vicinity of a disc-shaped ice particle or an hexagonal plate. The vapour density gradient favours growth from the edges of the plate over that from the faces, and growth from the corners where the gradient is strongest is even more favoured. On this basis, it would be difficult to explain the variety of crystal types occurring in natural snow. It is only when this distortion of the field is combined with the effect of curvature on surface vapour density that a suitable mechanism explaining growth habits can be introduced.

4.2 The Electrostatic Analogue

It will be shown in a subsequent section that for steady state diffusion the vapour density in space is given by the solution of Laplace's equation $\nabla^2 \rho = 0$, where ρ satisfies the boundary conditions at the surface of the particle and at infinity. Jeffreys (1918), in considering the transpiration process in plant life, set up an electrostatic analogue to calculate the overall rate of evaporation from leaves. This was first applied to the problem of growing ice crystals by Houghton.

Since the potential function V satisfies the Laplacian in electrostatics, vapour density and potential are interchangeable. Also the charge q on the body is equal to CV_o, where C is the capacity and V_o the surface potential. By Gauss' theorem,

$$\iint_S \frac{\partial V}{\partial n}\, dS = 4\pi q = 4\pi\, CV_o,$$

where S is the surface area of the body

and n the direction of the normal to the element of area dS.

The rate of evaporation from the body is then

$$\iint_S D\, \frac{\partial \rho}{\partial n}\, dS = 4\pi\, CD\, \rho_o, \qquad (4.1)$$

where D is the diffusivity.

Jeffreys assumed that the vapour density at the surface of the evaporating body was at some constant value ρ_0 and thus neglected curvature effects on equilibrium vapour density. His concept is a valuable one, however, permitting the calculation of total rate of mass transfer to or from odd shaped bodies if their electrostatic capacities are known. A further extension of the theory is necessary to investigate the effect, due to curvature, of the non-uniform surface vapour density on the rate of growth.

4.3 Electrodynamic Analogy

There is also close resemblance between the electrostatic field and the state of dynamic equilibrium represented by a steady flow of electric charge through a conducting medium.

If a hypothetical closed surface in the medium which does not enclose any sources is considered, then

$$\iint_S \bar{J} \cdot \bar{n} \, dS = - \frac{\partial q}{\partial t} \tag{4.2}$$

where $\bar{J}$ is the current density vector (rate of flow of electric charge per unit area),

n is the normal to the surface,

S is the area of the enclosing surface,

and $\frac{\partial q}{\partial t}$ is the rate of increase of charge within the surface.

Using the theorem of flux, the surface integral in equation (4.2) may be transformed to a volume integral. Thus

$$\iiint_V \operatorname{div} \bar{J} \, dv = - \iiint_V \frac{\partial q_v}{\partial t} \, dv, \tag{4.3}$$

where v is the volume enclosed by the surface, and

q_v is defined by $q = \iiint_v q_v dv$.

Or

$$\text{div } \bar{J} = -\frac{\partial q_v}{\partial t} \quad . \qquad (4.4)$$

For the steady state reached in conduction, q_v is a constant, so that

$$\iint_S \bar{J} \cdot \bar{n} \; dS = 0 \quad \text{and} \quad \text{div } \bar{J} = 0. \qquad (4.5)$$

If the conducting medium is isotropic,

$$\bar{J} = \sigma \bar{E} \qquad (4.6)$$

where σ is the conductivity,

and E the electric field vector.

In addition, if the medium is homogeneous, σ is constant and equation (4.5) reduces to

$$\text{div } \bar{E} = 0 \qquad (4.7)$$

$$\text{or} \qquad \nabla^2 V = 0 \quad , \qquad (4.8)$$

so that the potential satisfies Laplace's equation.

Consider now the total current i flowing to a body at potential V_o immersed in a conducting medium and surrounded by a spherical shell at a large distance from it and at a potential V_∞, where $V_\infty > V_o$. From equation (4.2)

$$i = \iint_S \bar{J} \cdot \bar{n} \, dS$$

$$= \frac{1}{\sigma} \iint_S \bar{E} \cdot \bar{n} \, dS$$

$$= \frac{1}{\sigma} \iint_S \frac{\partial V}{\partial n} \, dS. \qquad (4.9)$$

If the surface potential of the body is assumed constant, Jeffreys' result is reproduced. That is

$$i = \frac{1}{\sigma} \iint_S \bar{E} \cdot \bar{n} \, dS = \frac{4\pi C}{\sigma} (V_\infty - V_0). \qquad (4.10)$$

This theory, leading up to the end result (4.10), bears a closer similarity to diffusion theory than does the electrostatic case. For i, which is the rate of flow of charge, becomes $\frac{dm}{dt}$, the rate of mass transfer, and σ the conductivity is related to the diffusivity by $D = 1/\sigma$. It appears that a valuable method of measuring rates of growth or evaporation of irregular bodies (snow crystals) in the laboratory could evolve from this.

4.4 The Inhibiting Mechanism

From equation (4.9) it is seen that the rate of growth per unit area is proportional to the vapour density gradient. Thus for an oblate spheroid (a first approximation to an hexagonal plate) whose ratio of major to minor axes is 10:1, the growth per unit area along the edges is 10 times that along the flatter faces, since the gradients are in the same proportion. A diagram of the equipotentials (or lines of constant vapour density) around a disc is shown in figure 4.1, the last equipotential line being half of the value at infinity. A graph of vapour density (normalized) against reciprocal distance (figure 4.1) shows that the gradient is very much steeper at the perimeter of the disc than at its flat faces. The straight line is that corresponding to an equivalent sphere, since the radii of a disc and a sphere of equal capacities are in the ratio of $\pi/2$.

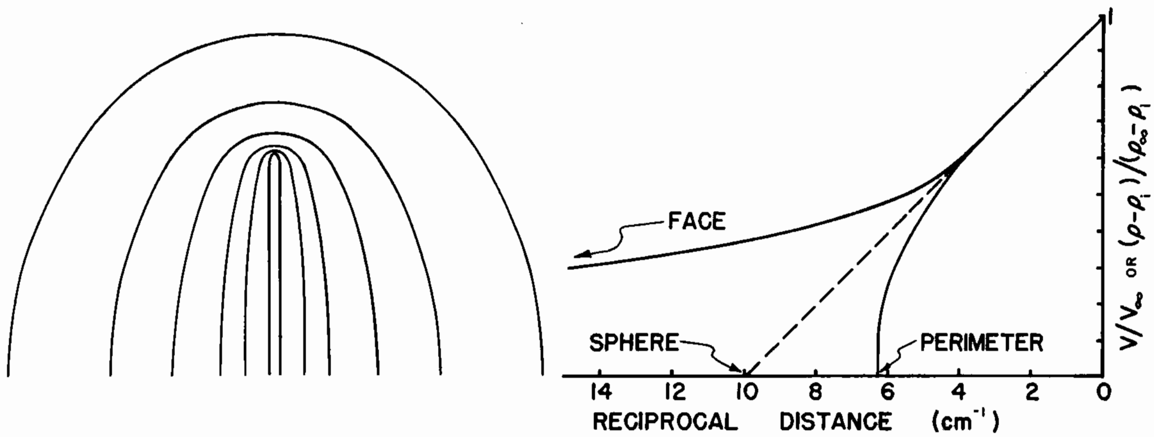

FIG. 4.1 - The equipotentials around a conducting disc are shown in equal steps of potential, the last being half the value at infinity. The gradient is much greater at the perimeter than at the relatively flat faces. At the right potential (or vapour density) is represented against reciprocal distance and illustrates the same feature. The straight line is that corresponding to a sphere whose capacity is equal to that of the disc.

The assumption has been made that the vapour density is constant at the surface of the body. The vapour density field around an hexagonal plate then favours continued growth as a thin plate. In fact, one would be led always to expect dendritic growth, since the gradient would be greatest at the corners and consequently the relative growth most rapid there.

If, however, the equilibrium vapour density is higher at the edges than over a flat surface, and that at the corners higher still, these otherwise-favoured types of growth will be inhibited until the excess of the ambient vapour density is of sufficient magnitude to overcome these inhibitions.

A somewhat similar situation is found in radio tube theory when operating at positive grid bias. When the grid bias becomes positive or if the anode voltage drops sufficiently, it is possible to have a large current flow from grid to cathode. Similarly, if the ambient vapour density decreases by a suitable amount, a mass flow could be expected from the perimeter of the crystal to the faces and transitions in crystal type occur.

<u>4.5 Electrolytic Tank Experiment</u>

A composite model of an hexagonal plate was made, a sketch of which is shown in figure 4.2 (left). It was composed of five sheets of aluminum foil, two acting as the faces, two cut to simulate the edges, and the central one the corners. Sheets of waterproofed paper, acting as insulators, were placed between the foil surfaces and the whole cemented together. The areas of foil exposed corresponded to the faces, edges and corners of the crystal. Electrodes were attached to the metal foils so that variable potentials could be applied to each. A spherical shell of aluminum foil, large compared to the dimensions of the crystal, surrounded the model and both were immersed in a tank of ordinary tap water.

With the experimental arrangement used, it was possible to apply different potentials on the faces, edges, corners and on the large shell which will be called infinity. Current measuring meters were included in series with the faces, the edges and the corners, and both voltage and current readings were taken simultaneously.

For easy interpretation of the results, a first set of observations was taken with the same potential being applied to both edges and corners (i.e. to the whole perimeter). The faces were always kept at ground potential and, for a given voltage on the perimeter, the potential applied to the distant electrode was varied and current readings were recorded. The results are illustrated by two sets of curves in figure 4.2, the set at 10 volts perimeter potential being typical of the data obtained when that potential was 5 and 20 volts. When any given potential was applied to the perimeter and the potential applied to the distant electrode gradually increased from zero, it was observed that at first there was a

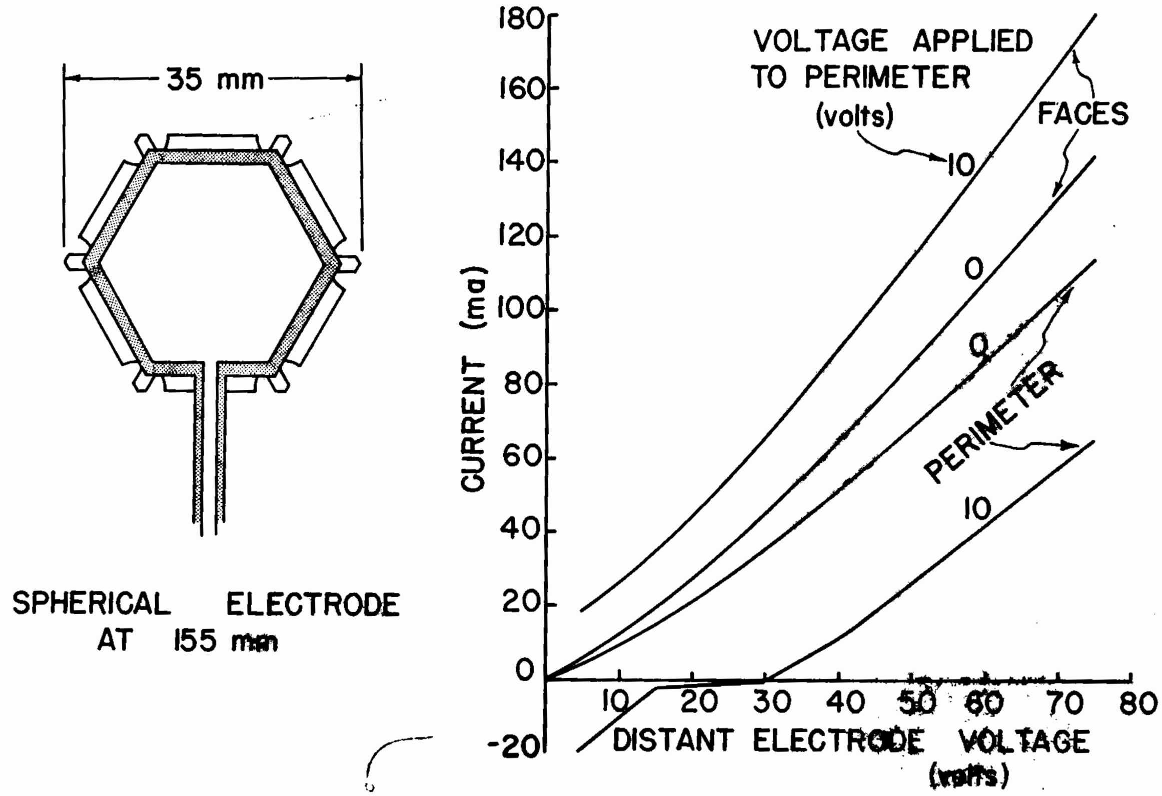

FIG. 4.2 - At left is shown a sketch of the crystal model used in the electrolytic tank experiment. To the right, current to the faces and perimeter of the model is plotted as a function of the voltage applied to the distant electrode for perimeter voltages of 0 and 10 volts.

current flow from the perimeter to the faces of the crystal model. This current flow from the perimeter decreased rapidly with increasing distant field, the current to the faces, however, increasing steadily with applied field. When the distant potential had risen to three times the perimeter potential there was no net flow to or from the perimeter. For higher values of potential applied to the distant electrode, the current to the perimeter increased rapidly, soon exceeding per unit area the flow to the faces. The effect on the total current of a voltage on the perimeter was equivalent to applying a voltage 0.3 times as great to the whole crystal. It is worth noting the anomaly shown by the curve of current to the perimeter against distant voltage in the region 15 to 30 volts when the perimeter potential was 10 volts (figure 4.2).

Referring these results to a curve of potential difference against reciprocal distance (figure 4.3), the perimeter is located some distance out from the radius of the equivalent sphere (capacity) towards the distant electrode which is near infinity. Since the electrode referred to as the perimeter had a finite width and since it was hexagonal in shape, the letters a and b designate the locations of the farthest and nearest points of the outside of the "perimeter", and c and d correspond to the inside of the "perimeter". The actual potential on the perimeter is indicated by the vertical extent of the arrowheads rising from these points. The equivalent sphere, as follows from the experimental results, has also been given a potential 0.3 times that of the perimeter. The slope of the locus represents everywhere the current flow per unit solid angle to the equivalent sphere. Pivoting the locus about the equivalent sphere

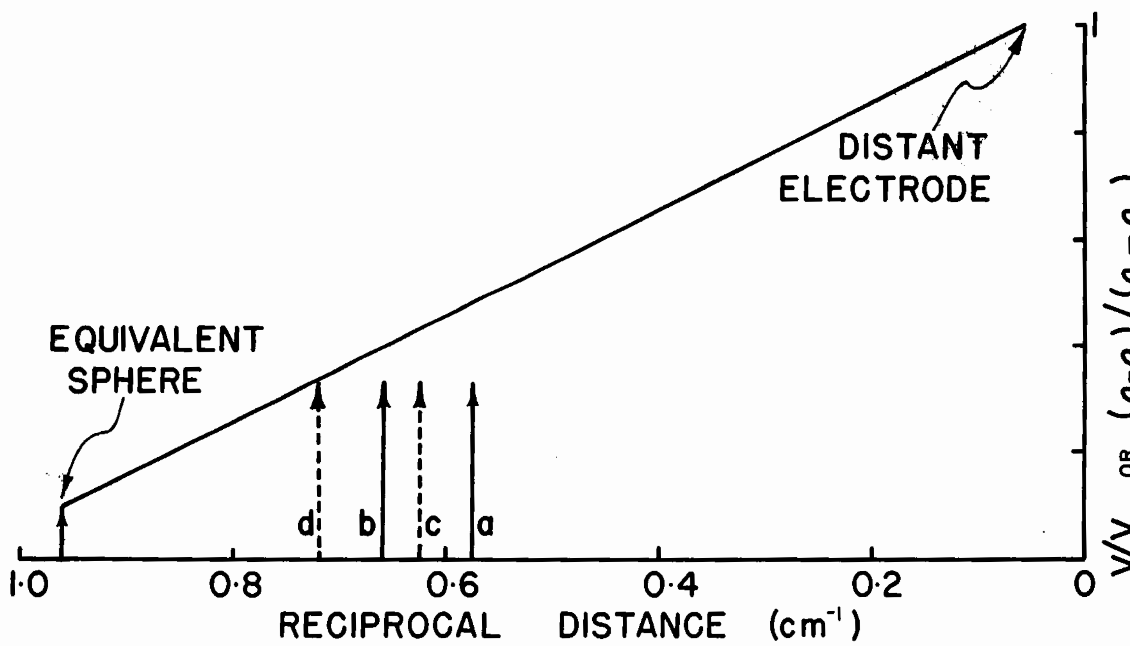

FIG. 4.3 - Potential, normalized against that of the distant electrode, is plotted against reciprocal distance. Using the dimensions of the "crystal" and of the distant electrode, the equivalent sphere is represented at the left, the arrowhead denoting its potential. The outside of the "perimeter" extends from a to b, the inner part from c to d. The potential assigned to the perimeter is one-third that of the distant electrode (being the critical case when the field value in the neighbourhood of the perimeter is near the potential on the perimeter).

corresponds to changing the potential of the distant electrode. It is seen that this moving locus would enter the region a to d of the perimeter arrowheads when the distant potential was 1.9 times that on the perimeter and leave that region when the factor was exactly 3. (The latter factor has already been shown to be the critical ratio of distant to perimeter potential for which there is no flow to or from the perimeter.) This would also explain the anomaly observed in the perimeter current, since with increasing applied field, the transition in perimeter current occurred between 15 and 30 volts when the perimeter voltage was 10 volts, giving almost the same factors as found from figure 4.3. It is then apparent that the distortion to the field around an equipotential disc, if a higher potential is applied to the perimeter, is only local. The distortion is in such a direction as to render the field more radial.

Further sets of experiments were performed to ascertain the corner effect. For this purpose, the faces were again kept at zero potential, the edges at 5 volts, and the corners at 10 volts. A somewhat similar effect was observed with respect to the corners, the current to the corners cutting off when the potential of the distant electrode was somewhat more than three times that on the faces. Interpretation was more difficult because of several complicating factors: a different water bath was used and electrolytic action and corrosion had attacked the crystal model, in particular at the corners which had begun disintegrating.

4.6 Mode of Crystal Development

The results of the electrolytic tank experiment can be transposed at least qualitatively to provide the mechanism necessary for transitions from one type of crystal growth to another.

Because the basic crystalline structure of ice is thought to be hexagonal, a reasonable form to assume for a snow crystal in its initial stages of growth is that of a tiny hexagonal plate. The future growth habit, however, would appear to depend on the nature of the diffusion field, and so on the vapour density excess.

The behaviour is intelligible when referred to figure 4.3 where vapour density excess is now the ordinate. An hexagonal crystal of uniform surface vapour density around its perimeter, which is slightly in excess of that over its faces, distorts the field locally, tending to make it more radial, but does little to the distant field. The coincidence of the field around the crystal and that of its equivalent sphere is presumably best when the perimeter has the field associated with the equivalent sphere at that point (almost as illustrated in figure 4.3). In any case, the vapour flow to the perimeter is proportional to the difference between the field value in the neighbourhood of the perimeter and the surface value on the perimeter.

In point of fact, considering an hexagonal snow crystal, the near edge is located approximately 0.32 of the way to infinity from the equivalent sphere, and the corners extend out to about 0.4, a little further into the diffusion field (figure 4.4). The surface vapour density at the corners is also slightly higher than that at the edges. If the ambient vapour density excess is small, both edge and corner growth are inhibited, actually

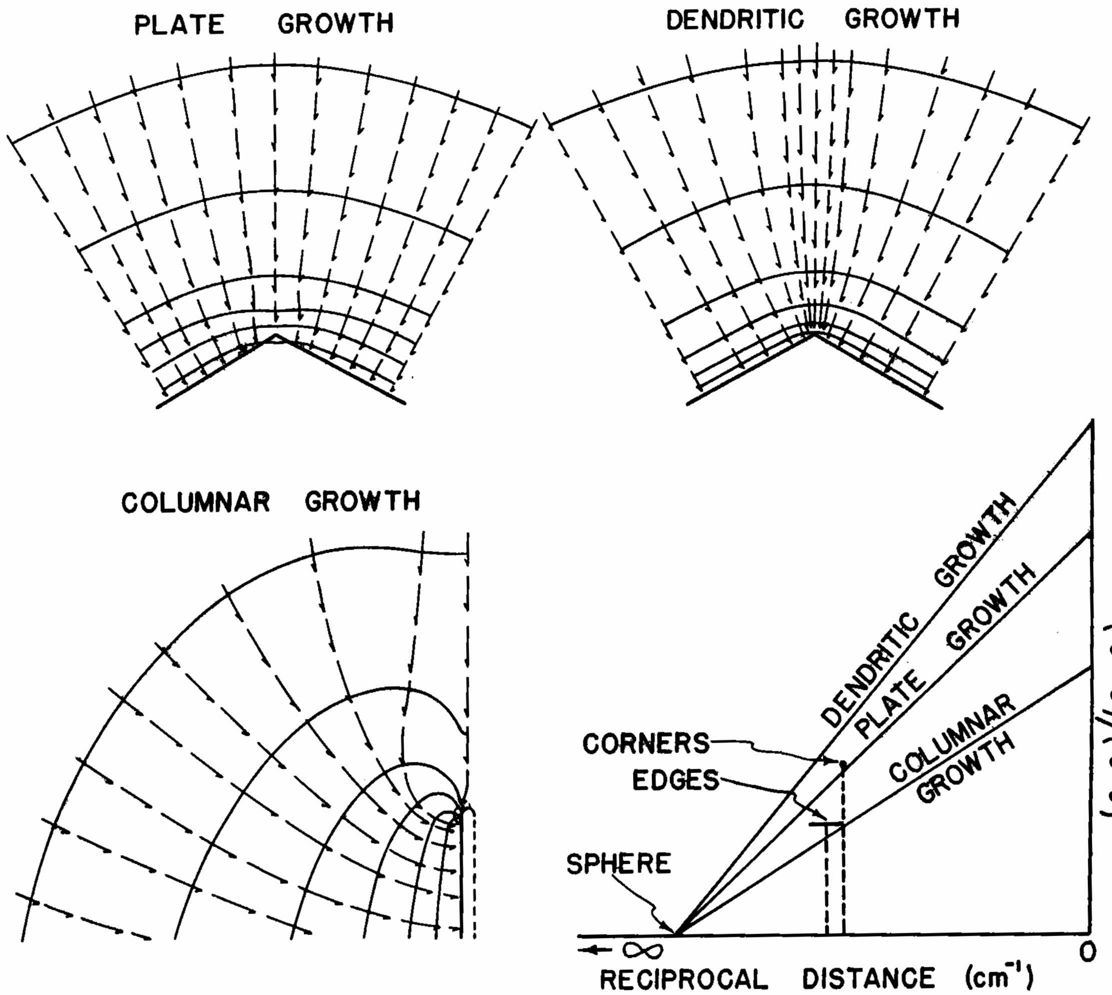

FIG. 4.4 - The lines of constant vapour density and the flow lines favourable for columnar, plate-like and dendritic growth are here illustrated. The transition from one type of growth to another is shown by the three curves of vapour density excess plotted against reciprocal distance.

made negative, and the crystal grows outward from its faces as a column (figure 4.4, bottom left). If the excess is sufficient to overcome the inhibition to edge growth, but not that to corner growth (figure 4.4, top left), the crystal grows as a plate while thickening only slowly. If the excess is greater again and sufficient to overcome the inhibition to corner growth, the crystal grows outward from its corners as a dendrite (figure 4.4, top right). Should the vapour density excess fall off momentarily at any stage in the growth of a dendrite, then each of the six branches broadens to provide the roots for a symmetrical array of leaves. These continue to grow when the crystal returns to corner growth, but more and more slowly as they become shielded by the principal arms. Similar leaves may, of course, result from the adherence to the branches of cloud droplets, but the leaves are not likely to be symmetrically disposed.

Our loci of constant $(\rho_v - \rho_i)$ on the Nakaya data (figure 3.2) illustrate this effect quite clearly. Decreasing this vapour density excess continuously, one passes through the dendrite region to that where thin plates are most prevalent, then on to thick plates and through to columns. Now the transition from columnar to plate-like growth (figure 3.2) occurs when the vapour density excess is 0.18 gm m^{-3}. Combining this with results from the electrolytic tank experiment for the critical point where flow to the perimeter has just ceased (the case shown in figure 4.3), it appears that the surface vapour density at the perimeter exceeds that on the faces by approximately 0.06 gm m^{-3},* and that no net growth can take place unless the excess of ambient over the effective ice crystal vapour density is greater than about 0.02 gm m^{-3}.** According to our analysis of the Nakaya data, however, no growth was reported for vapour

* It has been necessary to assume that the excess of the perimeter vapour density over that on the faces does not vary significantly with temperature. It is possible that the surface vapour density over curved solids differ in this respect from curved liquid surfaces.

** If our concepts are valid, this fact should be taken into consideration in calculating rates of growth of snow crystals, i.e. the rate of growth should be proportional to difference between the ambient vapour density and the surface vapour density of the sphere equivalent in capacity to the crystal, adjustments being made as well for the temperature of the growing crystal.

density excesses less than 0.1 gm m^{-3}, corresponding to a temperature limit of -4C. This discrepancy could be due to the difficulty of nucleation at temperatures warmer than -4C, or because the net growth (if any did result in the Nakaya experiment for $\Delta\rho < 0.1$ gm m^{-3}) did not produce a crystal of distinguishable form.

In summary then, it is suggested that the variety in the modes of crystal development can be suitably explained by means of the vapour density excess if a non-uniform surface vapour density at the crystal is assumed.

5. RATE OF GROWTH OF AN ICE CRYSTAL IN CLOUD

5.1 Introduction

The general diffusion equation of water vapour into air, assuming a uniform air density, is given by

$$\frac{d\rho}{dt} = \frac{\partial}{\partial x}\left(D\frac{\partial \rho}{\partial x}\right) + \frac{\partial}{\partial y}\left(D\frac{\partial \rho}{\partial y}\right) + \frac{\partial}{\partial z}\left(D\frac{\partial \rho}{\partial z}\right).$$

If the medium is such that the diffusion coefficient is independent of position, then

$$\frac{d\rho}{dt} = D\ \nabla^2\ \rho.$$

If the ice particle is at rest relative to its environment and after the diffusion field surrounding it has attained a steady state, $\frac{d\rho}{dt} = 0$. The vapour density at any point in space is then given by the Laplacian equation subject to suitable boundary conditions. These are usually, (a) at an infinite distance from the particle the vapour density ρ_w is at water equilibrium at the ambient temperature, and (b) at the surface of the particle the vapour density ρ_i is at equilibrium with ice at the temperature of the ice.

The rate of mass transfer $\frac{dm}{dt}$ across any spherical surface of radius r about the particle is proportional to the area of the surface, the vapour density gradient there, and the diffusivity of water vapour in air. In fact

$$\frac{dm}{dt} = -\ 4\pi r^2\ D\ \frac{d\rho}{dr}\ . \qquad (5.1)$$

Assuming the crystal to be spherical in shape and of radius a, and solving the spherically symmetric Laplacian

$$\frac{d^2\rho}{dr^2} + \frac{2}{r}\frac{d\rho}{dr} = 0 \qquad (5.2)$$

for the density gradient, the rate of growth $\frac{dM}{dt}$ of the particle is

$$\frac{dM}{dt} = \frac{dm}{dt} = 4\pi aD(\rho_w - \rho_i). \qquad (5.3)$$

The result (5.3) may be generalized to apply to any odd shaped bodies by using Jeffreys' analogy which was discussed in section 4.2. For a body of electrostatic capacity C, the rate of growth becomes

$$\frac{dM}{dt} = 4\pi CD(\rho_w - \rho_i). \qquad (5.4)$$

Since it is mathematically simpler to treat spheres and spherically symmetric fields, the rate of growth of a spherical particle will be considered with the assumption that the result will also hold for any body of equivalent electrostatic capacity.

5.2 Growth in Cloud

The simple treatment given thus far assumed that there were no sources of vapour present other than at infinity.

Now suppose that the particle is in the presence of supercooled water droplets. Let the cloud droplets be uniformly distributed throughout the volume and let $\sum_1 r_c$ be the sum of the radii of the drops per unit volume. We tacitly assume that the cloud drop size distribution does not change with the sampling volume, no matter how small it is.

The rate of evaporation for each cloud droplet is simply $4\pi r_c D(\rho_w - \rho)$*, where ρ is the vapour density in the vicinity of the drop after a steady state has been reached. Now the rate of evaporation from a shell of thickness Δr surrounding the ice crystal is proportional to the volume of the shell, i.e. to the summation of cloud drop radii in it. Thus the contribution from the shell is

$$\Delta\left(\frac{dm}{dt}\right) = 4\pi r^2 \Delta r \left[4\pi \sum_1 r_c D(\rho_w - \rho)\right] .$$

So that

$$\frac{d}{dr}\left(\frac{dm}{dt}\right) = 4\pi r^2 \left[4\pi \sum_1 r_c D(\rho_w - \rho)\right].$$

But the rate of mass transfer across any spherical surface about the ice particle was given by equation (5.1).

$$\therefore \qquad \frac{d}{dr}\left(-4\pi r^2 D \frac{d\rho}{dr}\right) = 4\pi r^2 \left[4\pi \sum_1 r_c D(\rho_w - \rho)\right] .$$

i.e.

$$\frac{d^2\rho}{dr^2} + \frac{2}{r}\frac{d\rho}{dr} - (\rho - \rho_w)\left(4\pi \sum_1 r_c\right) = 0. \qquad (5.5)$$

The differential equation (5.5) corresponds to equation (5.2), the extra term accounting for the added sources of vapour. It is to be noted that whereas the rate of change of mass transfer with distance was equal

* The following argument may serve to justify the assumption that the water drops (cloud) are all at the same temperature irrespective of their distance from the ice crystal (i.e. that we are able to use the same ρ_W). The ice crystal is releasing heat (the latent heat of sublimation) and a plot of temperature against distance from the crystal would be similar to the inverse of figure 5.1. The cloud droplets, however, are evaporating and are thus below the temperature of their immediate environment, the depressions becoming larger for drops closer to the crystal where the air temperature is higher. Thus the resulting drop temperatures are approximately equal as has been verified by rough calculations.

to zero for the first case discussed (i.e. the mass transfer was continuous from source to sink), this is no longer the case.

Substituting

$$x = (4\pi \textstyle\sum_i r_c)^{1/2}\, r = kr$$

into equation (5.5), a more symmetrical form results:

$$\frac{d^2\rho}{dx^2} + \frac{2}{x}\frac{d\rho}{dx} - (\rho - \rho_w) = 0. \qquad (5.6)$$

A solution to this equation is

$$\rho - \rho_w = A\,\frac{\cosh x}{x} + B\,\frac{\sinh x}{x}.$$

Now $\rho = \rho_w$ as x approaches ∞, and since $\cosh x = \sinh x$ for large x, we have that $A = -B$, i.e.

$$\rho - \rho_w = A\left[\frac{\sinh x}{x} - \frac{\cosh x}{x}\right].$$

But $\rho = \rho_i$ when $x = x_i$ (i.e. when $r = a$), so that

$$A = (\rho_i - \rho_w)\left[\frac{\sinh x_i}{x_i} - \frac{\cosh x_i}{x_i}\right]^{-1}.$$

The solution for the vapour density at any point in space is then

$$\rho = \rho_w - (\rho_w - \rho_i)\left[\frac{\sinh x_i}{x_i} - \frac{\cosh x_i}{x_i}\right]^{-1}\left[\frac{\sinh x}{x} - \frac{\cosh x}{x}\right]$$

$$= \rho_w - (\rho_w - \rho_i)\left[\frac{e^{-x_i}}{x_i}\right]^{-1}\frac{e^{-x}}{x}. \qquad (5.7)$$

This may be further simplified by making the substitution $x = Nx_i$ (or $r = Na$). The resulting expression for equation (5.7) becomes

$$\rho = \rho_w - (\rho_w - \rho_i)\, N^{-1}\, e^{-x_i\,(N-1)}. \qquad (5.8)$$

Equation (5.8) is perfectly general in nature so long as specific values are not assigned to the cloud temperature or the barometric pressure. These would define ρ_w and $\Delta\rho = \rho_w - \rho_i$ as discussed in section 2. The rate of mass transfer, being proportional to the vapour diffusivity, is also a function of temperature and pressure. Thus to retain generality in studying the effects of cloud, the equations will be put in a form dependent only on the dimensions of the ice particle and/or the dimensionless quantity $x_i = ka$, where $k = (4\pi \sum r_c)^{1/2}$ is some function of the cloud density.

To recapitulate and summarize, the relevant formulae are listed in table 3 for cloud-free air and in the presence of cloud.

Table 3

Formula	No Cloud	Cloud Present
$\dfrac{\rho - \rho_i}{\rho_w - \rho_i}$	$1 - \dfrac{1}{N}$	$1 - \dfrac{e^{-x_i(N-1)}}{N}$
$\dfrac{\frac{d\rho}{dr}}{\rho_w - \rho_i}$	$\dfrac{1}{N^2 a}$	$k\,\dfrac{e^{-x_i(N-1)}}{N}\left[1 + \dfrac{1}{Nx_i}\right]$
$\dfrac{\frac{dm}{dt}}{4\pi D(\rho_w - \rho_i)}$	a	$\dfrac{(Nx_i)^2}{k}\,\dfrac{e^{-x_i(N-1)}}{N}\left[1 + \dfrac{1}{Nx_i}\right]$
$\dfrac{\frac{d}{dr}\frac{dm}{dt}}{4\pi D(\rho_w - \rho_i)}$	0	$(Nx_i)^2\,\dfrac{e^{-x_i(N-1)}}{N}$

and at the surface of the growing ice particle

$\dfrac{\frac{dM}{dt}}{4\pi D(\rho_w - \rho_i)}$	a	$a(1 + ka)$

where N is defined by $r = Na$,

x_i is defined by $x_i = ka$,

and k is defined by $k = (4\pi \sum r_c)^{1/2}$.

5.3 Discussion of Results

It is of interest to examine the vapour density field as a function of radial distance from the ice particle. Curves representative of this are shown in figure 5.1 for ice spheres of radius 0.005 and 0.1 cm. The distance scale used has in each case been extended out to 15 times the radius of the particle. It is seen that the presence of cloud becomes much more significant as the particle size increases. For a given particle size, the higher the factor k (a measure of the cloud density) the sooner does the vapour density approach its water equilibrium value.

Consider now the rate of mass transfer. In the absence of cloud, there is a diffusion of vapour towards the ice sphere such that the mass flowing inward across every concentric spherical surface is the same. The presence of cloud modifies this picture, since any shell of finite thickness adds a contributing region to the vapour density. If $\frac{d}{dr}\left(\frac{dm}{dt}\right)\Big/\frac{dM}{dt}$ (the ratio of the rate of change of mass transfer across any spherical surface to the total mass transfer or rate of growth) is plotted against r, the resulting graph will show the relative contribution of the total mass transferred as a function of the distance from the ice particle. Two such curves are given in figure 5.2 for an ice sphere of radius a = 0.1 cm, and for cloud such that k = 1 and 5.5 cm^{-1}. The area under each curve is unity. For k = 5.5 cm^{-1}, the peak is at a much higher value and nearer to the particle, and the contribution from regions for which $r > 1.5$ cm. is negligible. When k = 1 cm^{-1}, the mass contribution is significant from regions as far out as 6 cm. This would indicate that, because of the larger reservoir of water available with increasing k, the particle is able to draw more vapour from closer in. Also for k = 0 the vapour is drawn from infinity.

The rate of growth, as is to be expected, also increases with k. Using $\frac{dM}{dt}/4\pi D(\rho_w - \rho_i)$ as ordinate in figure 5.3, so as to be independent of atmospheric variables, rates of growth are plotted as loci of constant k. The abscissa, using Jeffreys' analogy, is the electrostatic capacity C of the ice crystal (C = a for a sphere). The curve in the absence of cloud is a straight line of 45° slope passing through the origin. With increasing k, the curves all converge at the origin but lie above the straight line and show more and more pronounced curvature. Even a slight trace of cloud ($k = 1\ cm^{-1}$) increases the rate of growth appreciably (10% for C = 0.1 cm, 5% for C = 0.05 cm). Figure 5.3 can be replotted using as ordinate $\frac{dM}{dt}/4\pi CD(\rho_w - \rho_i)$ or the ratio of rate of growth in cloud to that without. The loci of constant k are now the straight lines given in figure 5.4.

An attempt has been made to relate the quantity $k = (4\pi \sum_i r_c)^{1/2}$ to typical cloud densities. The cloud drop size distributions of Weickmann and aufm Kampe (1952) of relatively young cloud show some uniform properties. The median radii are about 7μ and the root mean cube radii about 8μ. Assuming these two values, a relationship is obtained between liquid water content M_c ($gm\ m^{-3}$) and k (cm^{-1}). Very approximately, $M_c = 0.25\ k^2$. The cloud data of Diem (1948) however, have distributions which are much less uniform. The very rough relation found between M_c and k ($M_c \approx 0.14\ k^2$) may be out by as much as a factor 4.

It should be emphasized that all present methods of cloud sampling, such as slide techniques, discriminate against droplets of less than

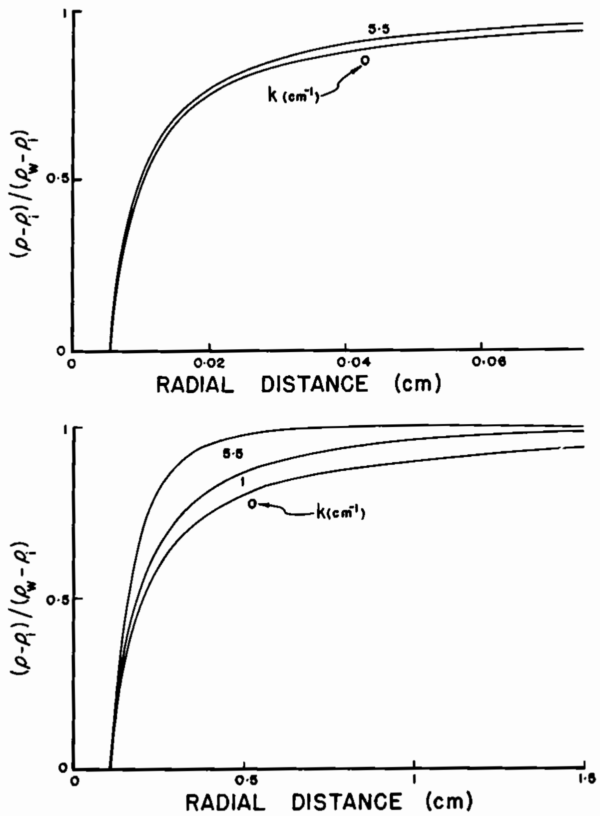

FIG. 5.1 - The vapour density field about an ice sphere growing by diffusion and sublimation is shown as a function of radial distance for spheres of radii 0.005 and 0.1 cm. For the smaller particle, cloud is not as significant as for the larger, the curve for $k = 1\ cm^{-1}$ in the upper diagram almost coinciding with that for $k = 0$.

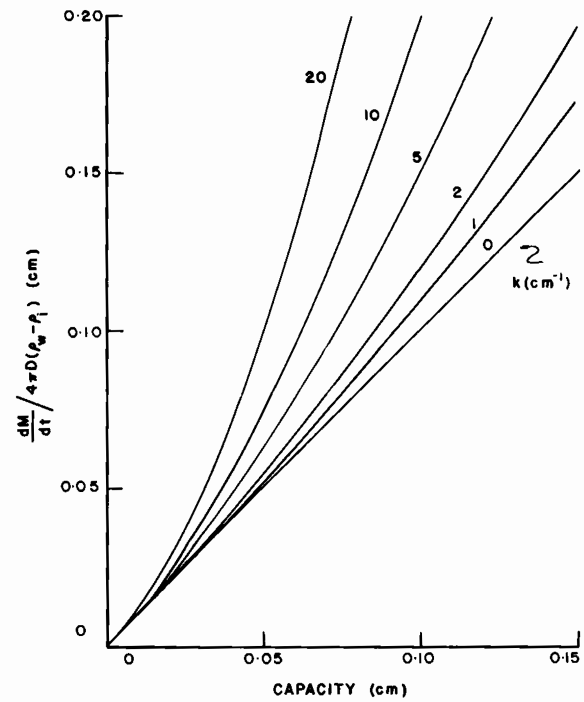

FIG. 5.3 - Curves representing rates of growth are plotted as loci of constant k and as a function of the electrostatic capacity of the crystal. The ordinate used is independent of atmospheric variables.

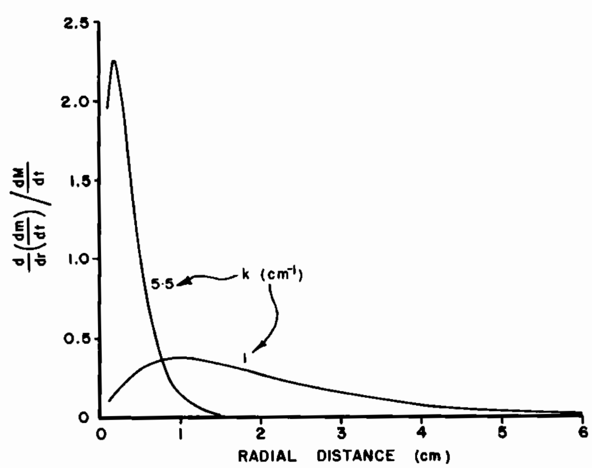

FIG. 5.2 - The contribution to the total mass transferred to the growing ice particle is shown as a function of distance from the particle for an ice sphere of radius 0.1 cm and for cloud of k factors 1 and 5.5 cm^{-1}. These have been normalized so that the area under each curve is unity.

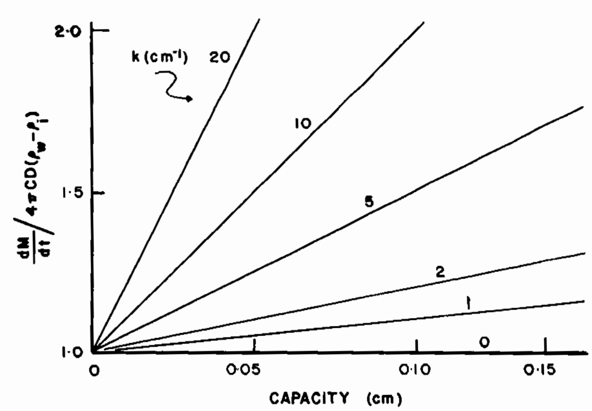

FIG. 5.4 - Rate of growth in cloud, relative to that in cloud free air, as a function of the electrostatic capacity of the crystal is plotted for various k values.

5μ diameter. This is readily admitted by most investigators who explain the abrupt cutoff at the lower limit by assuming that the smaller droplets are carried around the exposed slide by the streamlines which diverge there. The discrimination against these small cloud droplets, which are doubtless very numerous, makes no significant change in the liquid water content of the cloud which is proportional to the cube of the radii. The factor k (proportional to $r_c^{1/2}$) could however be appreciably increased. A cloud of, say, 2μ diameter drops, having a liquid water content of 1 gm m^{-3} (which is not unreasonable) would have a k factor such that $k^2 = 300$ cm^{-2}, and could enhance the rate of growth tremendously as the ice crystal increased in size. Thus better cloud drop spectra are needed before a fair evaluation of this process can be made.

If the vapour density field around a sphere is plotted against reciprocal distance from the sphere, a straight line results for the case of no cloud as is evident from the first formula in table 3. This has already been shown in figure 4.1 and the reciprocal scale usage has proved invaluable to the interpretation of the electrolytic tank experiment reviewed in section 4. It has further been found possible to approximate a cloud of given k value by a water shell whose radius r_w depends on k alone (i.e. the infinity boundary condition has been moved in to a distance r_w from the ice particle). The relationship between k and r_w^{-1} is shown in figure 5.5. For ice spheres of dimensions such that $a^{-1} > 10$ cm^{-1}, the vapour density field using the above approximation is essentially unchanged from the exact solution in the region for which $r^{-1} > 5$ cm^{-1}, where r is the distance from the ice particle. In the region $0 < r^{-1} < 5$ cm^{-1}, the approximate solution diverges from the exact one which is tending to $r^{-1} = 0$ as ρ approaches ρ_W, the divergence increasing with increasing k or a.

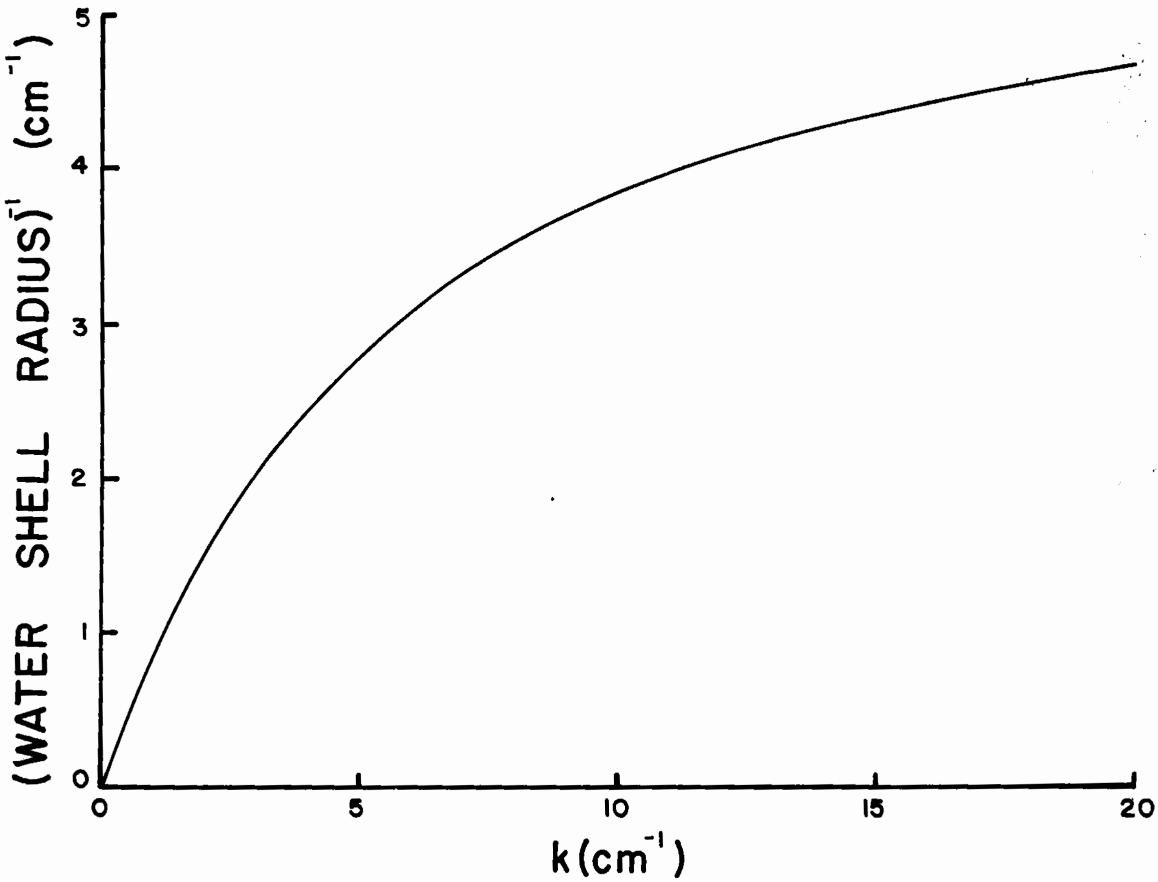

FIG. 5.5 - This relates the radius r_w of a water shell which would effectively replace a cloud of value k so that the vapour density field is essentially unchanged for $r^{-1} > 5$ cm^{-1} and ice spheres such that $a^{-1} > 10$ cm^{-1}.

The relative influence of cloud and supersaturation on crystal habit can now be compared. Consider first an atmosphere at -15 C and relative humidity of, say, 102%. The excess of the ambient vapour density over that at the surface of a growing ice particle after the latter has been corrected for temperature is about 1.23 times greater for the 2% of supersaturation than for an atmosphere at water equilibrium. The effective vapour density drop is thus increased by 1.23, this increase being independent of particle size. Approximating cloud by a water shell corresponds to having the water equilibrium boundary condition at some finite distance from the ice particle (figure 5.5).

This in turn leads to an effective vapour density at infinity which varies with the size of the particle. It is only when the particle attains appreciable dimensions and the cloud is dense that the effective vapour density excess is significantly greater than for an atmosphere at water equilibrium. Thus when $k = 10\ cm^{-1}$ the factor is 1.001 for a 10μ diameter ice particle, 1.02 for a 100μ particle and 1.23 for a 1000μ particle. It was because of this variability with size that the density in excess of water equilibrium in the form of vapour was used in section 3 in the analysis of the Nakaya data. The loci of constant $(\rho_w - \rho_i)$ in figure 3.2 are thus valid except at high cloud densities. At high cloud densities the locus bounding a crystal type domain would tend to spread so as to include the few dendrites and plates which had been missed previously.

Ventilation or relative motion between the ice crystal and its surroundings has been neglected in this study. The difficulties inherent in a theoretical approach to this problem are formidable. Experimental results by Frossling (1938), Gunn and Kinzer (1951), and Houghton and Radford (1938) on ventilated evaporating water spheres are all in conflict. Presumably ventilation plays a role somewhat similar to cloud in that it brings the defining boundary in from infinity closer to the particle. The rate of growth of ice crystals is thus enhanced by ventilation.

5.4 Size Attained by Growing Ice Crystals in the Atmosphere

The co-existence in the atmosphere of water in all its three phases, as in a mixed ice-water cloud, may lead to the growth of the ice crystals by direct sublimation of water vapour. If growth by accretion is not considered, the water drops act only as sources of vapour providing the vapour density gradient necessary for the growth of the ice crystals.

The final mass attained by a growing snow crystal will depend on its initial dimensions (or mass) and on its rate of growth. The depth of the cloud and the velocity of fall of the crystal relative to its environment will dictate the time available for the particle to grow.

Houghton has calculated rate of growth as a function of particle mass where the velocity factor has been included. As a most favourable case, he chose a temperature of -15C and a water saturated atmosphere. These are conditions suitable for dendritic growth and his results are shown in figure 5.6. Taking the initial mass of the ice crystal as 0.033 μgm and integrating his curve of rate of growth as a function of particle mass, he obtained a curve of mass against elapsed time which is reproduced in figure 5.7. It shows that an ice crystal growing by sublimation under the conditions stated could attain a mass of about 500 μgm in about 60 min after falling approximately 1 kilometre, thus resulting at best in a drizzle drop (if melted).

Making the same basic assumptions as Houghton regarding the air temperature, type of crystal growth, initial mass, and relative velocity we have gone through a similar procedure of calculating rate of growth as a function of particle mass with the exception that the growth was considered in the presence of cloud. A factor $k = 10\ cm^{-1}$ was chosen as equivalent to a moderate cloud and the results plotted in figure 5.6. The integrated curve yielding mass against elapsed time is compared to Houghton's in figure 5.7. The divergence between the two increases rapidly with time. After 10 min have elapsed, the crystal growing in

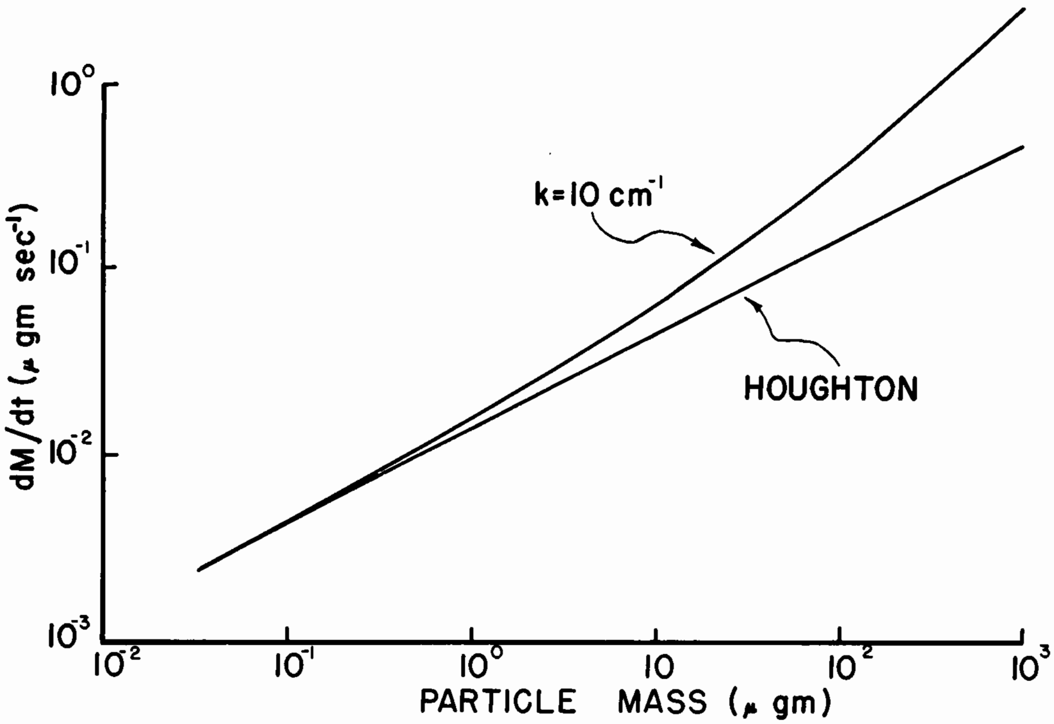

FIG. 5.6 - Houghton's curve of rate of growth as a function of particle mass is compared to the present calculations for a moderate cloud.

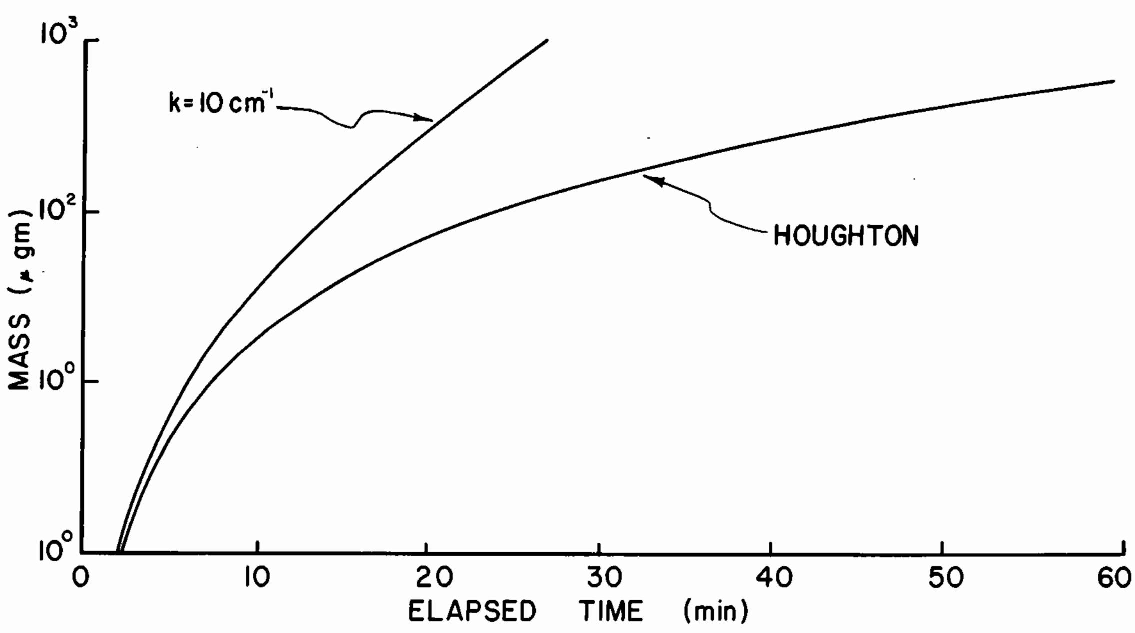

FIG. 5.7 - Starting with an ice crystal of mass 0.033 μ gm and integrating the curves of figure 5.6, the mass attained is shown against elapsed time.

cloud is 2 times the mass of that growing at water saturation; after 20 min the ratio is about 4; after 30 min, about 8. Also the mass attained at water saturation in 60 min can be exceeded in less than 25 min in this cloud.

It would appear that cloud enhances the sublimation process. When Houghton's curves of growth by sublimation are modified by these considerations, they can explain the larger ice crystals that are observed (i.e. about 1000 μ gm on the basis of a time of growth in the cloud of the order of half an hour or less). This does not imply that precipitation particles equivalent to fair sized raindrops normally result from the sublimation process alone. One must still consider growth by accretion and the bunching of many crystals into aggregates to account for the large size rain drops observed.

6. CONCLUSIONS

The distribution of snow crystal types as a function of temperature observed by Nakaya and Hanajima suggests symmetry about the maximum of a curve of $\rho_w - \rho_i$ against temperature, where ρ_w is the vapour density at equilibrium with water at the air temperature and ρ_i is the ice equilibrium value at the temperature of the growing ice particle which is slightly warmer than the air temperature. Starting from this clue, attempts were made to explain the whole of the Nakaya distribution as depending primarily on the excess of the ambient vapour density over that at the surface of the growing ice crystal. This attempt was successful when it was assumed that the excess water above the liquid equilibrium value in Nakaya's experiment consisted largely of water cloud but in small part of supersaturated vapour. While the presence of fine water cloud affected the vapour density gradient at the surface of the growing ice particle, the effect varied with particle size, and except for very large particles, it appeared that the small amount of true supersaturation was more significant than the presence of cloud in influencing the type of growth in that experiment.

A simple analytical expression was derived for calculating $\Delta\rho$ as a function of temperature. It was found that, although the psychrometric values were directly proportional to the atmospheric pressure, the $\Delta\rho$ values were a much less sensitive function of the pressure. In order to explain crystal habit at high altitudes (i.e. low barometric pressures), it seems necessary to modify the $\Delta\rho$ curves by the ratio of standard to existing pressures taken to a power of about 0.3. The exact figure 0.286, which occurs in the definition of potential temperature, caused the curves to assume the same peak value. We have been unable to find any physical basis for this coincidence. The shift towards lower temperatures with decreasing pressure as was observed by Gold and Power for any given crystal type was then in good agreement with these modified curves.

In the course of analysing Nakaya's data, a plausible mechanism explaining the dependence of crystal habit on vapour density excess suggested itself. Since equilibrium vapour density over liquids is a function of the curvature of the surfaces, this was also postulated for snow crystal surfaces. An hexagonal snow crystal (plate) would then have a surface vapour density at its edges which exceeded that over its flat faces, and the corners being doubly rounded would have a still higher value. Growth to the corners and edges would be inhibited until the ambient vapour density was sufficient to overcome these inhibitions. This was verified in an electrolytic tank experiment using a model of an hexagonal snow crystal consisting of a set of electrodes at different potentials representing the faces, edges and corners of the crystal and applying a distant field. The results indicated that marked transitions occurred in the current per unit area flowing to the different electrodes as the distant field was increased. At first the flow was mainly to the faces, but, for a sufficiently high applied distant potential, flow to the edges was favoured and finally the flow per unit area to the corners exceeded the others. Columns result from diffusion to the faces, plates from edge growth and dendrites when the growth is from the corners. Crystal habit was thus explained by means of the existing vapour density excess in its ability to overcome the inhibitions mentioned.

The steady state diffusion equation was solved for an ice particle growing in the presence of cloud, the solution of the vapour density field being in terms of a parameter k which was proportional to the square root of the sum of the radii of the cloud droplets per unit volume. It was shown that with increasing k the ice particle could draw more vapour from closer in. A moderate cloud could thus enhance the rate of growth appreciably when the particle attained significant size. A growth curve in cloud as a function of elapsed time was calculated and compared to a similar curve of Houghton's where the growth was assumed to take place in a water saturated atmosphere. The cloud enhanced the diffusion and sublimation processes to such an extent that the time of growth from 0.033 μgm to 500 μ gm was reduced roughly by a factor of 3. Thus, though supersaturation rather than cloud was shown to be the dominant factor in the Nakaya experiment, clouds are probably important under natural conditions, because of their effect on larger crystals, in achieving in a reasonable time the large crystals observed at the ground.

References

August, E.F., 1825: Uber die Verdunstungskalte und deren Anwendung auf Hygrometrie. Ann. Physik, 5, 69-89.

aufm Kampe, H.J., Weickmann, H.K. and J.J. Kelly, 1951: The influence of temperature on the shape of ice crystals growing at water saturation. J. Meteor, 8, 168-174.

aufm Kampe, H.J. and H.K. Weickmann, 1952: Particle size distribution in different types of clouds. Proc. 3rd Radar Weather Conference, McGill University, Montreal, B 9-12.

Berry, F.A., Bollay, E. and N.R. Beers (eds.), 1945: Handbook of Meteorology New York, McGraw-Hill, 1068 pp.

Diem, M., 1948: Messungen der Grosse von Wolkenelementen II. Meteor. Rdsch. 1, 261-273.

Ferrel, W., 1886: Report on vapour tension, dew-point, and relative humidity tables. Annual Report, Chief Signal Officer, App. 24, 233-259.

Frossling, N., 1938: Uber die Verdunstung fallender Tropfen. Gerlands Beitr. Geophysik, 52, 170-216.

Goff, J.A. and S. Gratch, 1946: Low-pressure properties of water from -160 to 212°F. Trans. Amer. Soc. Heat and Vent. Eng., 52, 95-121.

Gold, L.W. and B.A. Power, 1952: Correlation of snow crystal type with estimated temperature of formation. J. Meteor, 9.

______________________, 1953: Dependence of natural snow on meteorological conditions. Submitted to J. Meteor. for publication.

Hanajima, M., 1944: Supplementary to "On the conditions for the formation of snow crystals" (in Japanese). Kisho Shushi (Mag. Met. Soc. Japan), 22, 123-127.

Houghton, H.G. and W.H. Radford, 1938: On the local dissipation of natural fog. Pap. Phys. Ocean. Meteor. Mass. Inst. Tech. and Woods Hole ocean. Instn, 6, No. 3, 63 pp.

Houghton, H.G., 1950: A preliminary quantitative analysis of precipitation mechanisms. J. Meteor., 7, 363-369.

Howell, W.E., 1949: The growth of cloud drops in uniformly cooled air. J. Meteor, 6, 134-149.

Ivory, J., 1822: On the hygrometer by evaporation. Phil. Mag., 60, 81-88.

Japanese papers, 1934-40: Physical investigations on snow. J. Fac. Sci. Hokkaido Imp. Univ., Sapporo, Japan, Vol. 1, 13 papers.

Jeffreys, H., 1918: Some problems of evaporation. Phil. Mag., 35, 270-280.

Kinzer, G.D. and R. Gunn, 1951: The evaporation, temperature, and thermal relaxation-time of freely falling waterdrops. J. Meteor, 8, 71-83.

List, R.J. (ed.), 1951: Smithsonian Meteorological Tables. Washington, Smithsonian Instn., 527 pp.

Mason, B.J., 1953: The growth of ice crystals in a supercooled water cloud. Quart. J. Roy. Met. Soc., 79, 339, 104-112.

Maxwell, J.C., 1879: On stresses in rarified gases arising from inequalities of temperature. Phil. Trans. 170, 231-256.

Montgomery, R.B., 1947: Viscosity and thermal conductivity of air and diffusivity of water vapour in air. J. Meteor, 4, 193-196.

Nakaya, U., 1938: Artificial snow. Quart. J. Roy. Met. Soc., 64, 277, 619-624.

__________, 1951: The formation of ice crystals. Compendium of Meteorology (Boston, Mass., Amer. Meteor. Soc.) 207-220.

Washburn, E.W., 1924: The vapour pressure of ice and water below the freezing point. Monthly Weather Review, 52, 488-490.

Wexler, R. and R.J. Boucher, 1952: Heat balance of a growing ice crystal. Mt. Washington Observatory, Scientific Report No. 2, under USAF Contract AF 19(122)-399.

PART II

MEASUREMENT OF THE TERMINAL VELOCITY AND MASS OF SNOWFLAKES

1. INTRODUCTION

Snowflakes, as observed at the earth's surface are usually found to fall in the form of aggregates of many individual crystals. It has been thought that snow, originating as single crystals, could fall considerable distances before aggregating, the clusters being produced by the collision and adhesion of the crystals during their course of fall when the temperatures were sufficiently high. Radar observations (Part III) suggest that on occasion, when the snow is generated in compact cells, aggregation may occur within these generating cells. Thus a relatively complex picture may exist, aggregation taking place at the generating level and again when the temperatures approach the melting point, with secondary processes possibly being in effect throughout the fall of the snowflakes.

There is a need for velocity information to interpret radar studies. Schaefer (1947) and Nakaya and Terada (1935) have measured the velocity of single crystals, but the behaviour of aggregates must be studied if aggregate flakes occur over a much wider range of heights than previously thought. A method was therefore developed whereby the mass and velocity of descent of snowflakes could be determined simultaneously.

Interpretation of radar information requires a knowledge of the size distribution of snowflakes as well, and a sample in space can be related to a sample collected at the ground by knowing velocity as a function of size. Dr. K.L.S. Gunn has attempted to obtain snowflake velocities as a function of size by sampling (a) through gravitational settling and (b) by sweeping out a volume of space. The velocities obtained from a comparison of the two suggested that the space distributions found by this method were not reliable, and so a more direct method has been used.

2. METHODS OF MEASUREMENT

2.1 Velocity of Fall

The velocity of fall of a particular snowflake was measured directly from the time interval taken for it to fall through a given vertical distance. The snowflakes were photographed in motion against a dark background from a distance of about 10 feet using a 16 mm movie camera. Each snowflake produced a short streak (due to its motion during the short time interval for which the lens shutter was open) on every frame of the film (figure 2.1). A camera speed of 32 frames

Figure 2.1 - A single exposure showing the vertical streaks made by the falling snowflakes.

per second, giving a measure of the time of fall, was found most suitable for successful registration of the streaks on the film. At this speed, the streaks were not too long and the natural illumination available was sufficient so that film of normal contrast could be used. The camera speed was carefully checked before and after the winter's operations by means of a stroboscopic flash unit and was found to be reliably constant.

Since the observations were taken in the open air, the camera recorded the snow falling between it and the dark background in the conical volume bounded by the angle of the camera lens. Snowflakes close to the camera, not being in the focal plane, produced very large blurred images on the film and tended to obliterate flakes which were more distant from the camera. It was thus found necessary to mount a stereoscopic attachment in front of the camera lens. In essence, this attachment* consisted of two systems of reflecting mirrors and prisms which viewed the field from a distance of about 2.75 inches apart. Two images were thus obtained from slightly different angles side by side on the 16 mm film. With this system, the more distant an object is from the camera, the more closely do its images occupy the same relative position on the split movie frame. A snowflake falling very close to one side of the stereo-attachment would still permit the other to obtain an unobstructed view (figure 2.2).

Figure 2.2 - The large blurred image at the left is caused by a snowflake falling close to the left aperture of the stereo-attachment.

Measurements were only made on the snowflakes which landed on the horizontal wool disc shown in figures 2.1 and 2.2. The films, after processing, were projected through a special type of projector** which could move the film, frame by frame, with perfect registration, as slowly as desired. The streaks due to a falling snowflake could then be followed on successive frames until it settled on the disc (sequence figure 2.3). Thus a velocity could be associated with a given flake on the disc. Minor corrections were applied to the velocities depending on the position of the flake on the disc (i.e. on its distance from the camera) and also if the snowflake was not falling in a plane parallel to the focal plane.

* Nord 3rd Dimension Converter, The Nord Co., Minneapolis, Minn.
** Dunning Animatic Projector, Dunningcolor Corp., Hollywood, Calif.

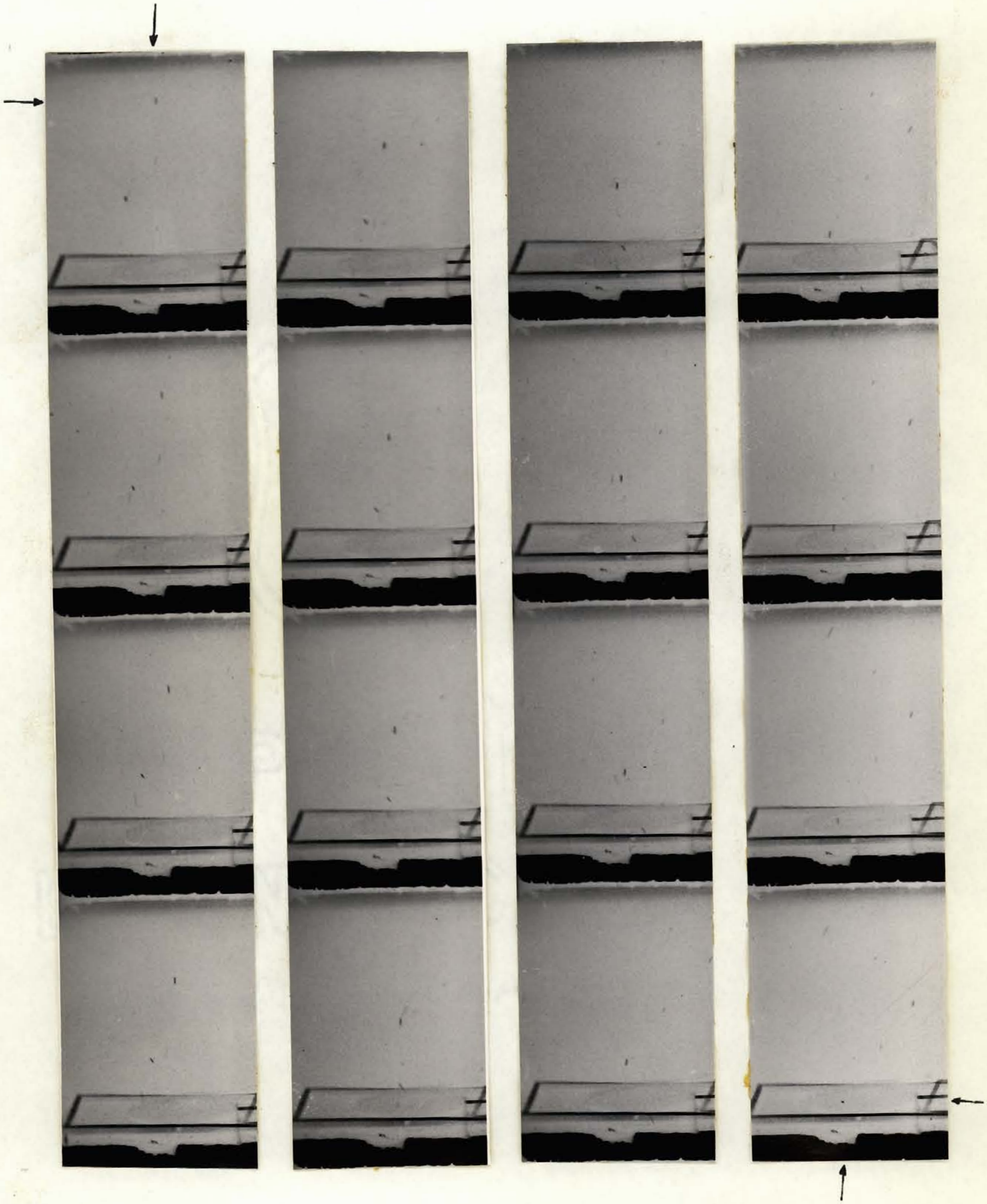

Figure 2.3 - A sequence of 16 consecutive exposures showing a snowflake gradually settling onto the horizontal wool disc. For ease of illustration, a very light snowfall has been chosen.

2.2 Melted Diameter and Crystal Types

The relevant snowflakes were those which settled onto the black angora wool disc, 13 inches in diameter. This disc, which was sheltered from further exposure to the snowfall when the camera was stopped, was then taken indoors. A Whatman #1 filter paper, previously dusted with powdered dye, was placed on the disc and absorbed the water from the melted snow particles. The calibration curve of Marshall, Langille and Palmer* (1947) was then used to relate the size of a stain on the filter paper to the diameter of the water drop equivalent in mass to the snowflake.

This diameter, which will be called melted diameter, is of significance for two reasons. a) The mass of the snowflake is proportional to the cube of this diameter whereas if the actual dimensions of a flake were considered, the relation between mass and dimensions would in general be more complex depending on crystal type, density and so on. b) It is also one of the significant quantities in radar theory where the back-scattered intensity is proportional to the sum of the sixth powers of the diameters per unit volume of space.

A correspondence was thus obtained between velocity and melted diameter. Closely spaced observations were also made of the crystal types forming the aggregates and on the state of aggregation, and temperatures at the ground were recorded.

---

* This calibration curve was carefully checked at frequent intervals within the melted diameter range of 0.08 to 0.5 cm. The method found most convenient was to place a small water drop on a waxed glass slide. The drop assumed the shape of a perfect hemisphere when the glass slide was horizontal. Its diameter was measured with a travelling microscope and related to the diameter of the stain which it produced on the filter paper.

3. OBSERVATIONS AND RESULTS

Before proceeding to a presentation of the results some statements will be made regarding the difficulties of obtaining usable observations and the consequent interpretation of the results.

a) On many occasions it was found that the air temperature at the ground during a snowfall rose to a value which could be a few degrees above the freezing point. Thus slight melting must have occurred and the aggregation would be more efficient under these conditions. Velocity measurements on such occasions would not be representative of snow velocities at temperatures below freezing.

b) On some of the days when temperatures were below the freezing point, severe winds approaching blizzard conditions were present. Sudden ground gusts in the vicinity could make the measurements unreliable.

c) The photographic method depended on the light scattered by the individual snow aggregates. Thus larger aggregates, having greater scattering cross-sections, were more easily registered on the film. The lower limit of detection was for melted diameters of about 0.04 cm.

d) Indirectly there was also discrimination between crystal types. For instance, in a snowfall containing dendrites and plates, the dendrites would be more efficiently photographed near the limit of detection since, for a given mass, the dendrites being less dense have a higher scattering cross-section than the plates.

e) Finally although the size distributions (see figure 3.1) are such that the numbers are highest for very small diameters and relatively few for large diameters, the efficiency of the velocity measurements increased with the size of the aggregates. Thus the number of velocity measurements within any diameter interval is not indicative of the

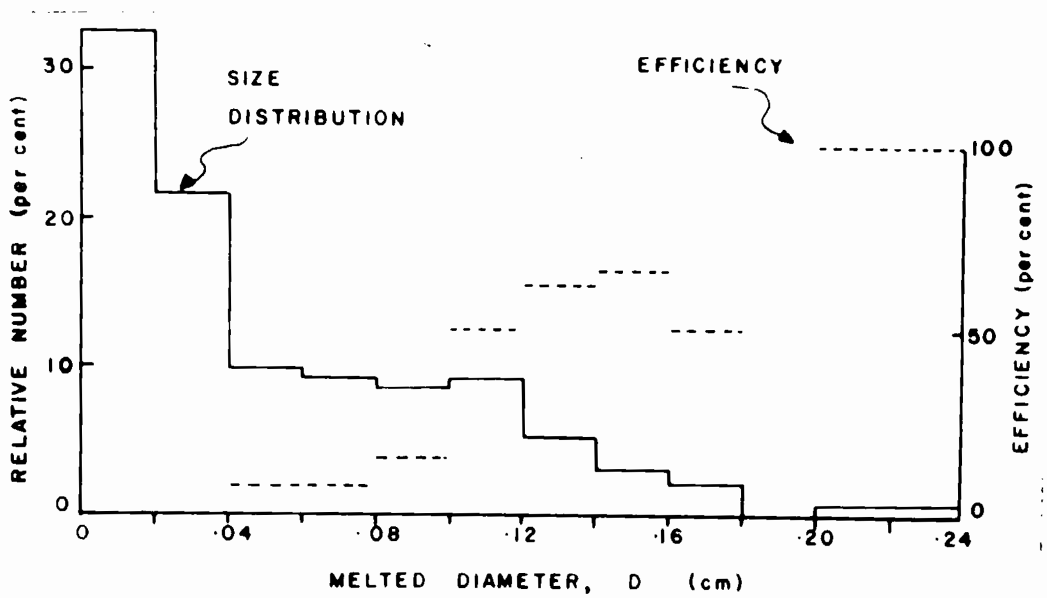

Figure 3.1 - A histogram for a typical case in which the ordinate is representative of the number of particles within the diameter intervals shown. The broken lines indicate the efficiency of the photographic technique as a function of particle size in this particular case.

total number in that interval. The efficiency (i.e. the ratio of the number of aggregates successfully photographed within a given diameter interval to the total number within that interval as collected on the horizontal wool disc) is shown for a typical case by the dotted lines in figure 3.1.

During the winter 1952-53, successful measurements were made on six days. When the data were plotted as logarithm of the velocity against logarithm of the melted diameter, it was found that for any given snowfall all the points, neglecting slight scatter, appeared to lie along a straight line and could thus be fitted within the range of measurement by an equation of the type

$$v = kD^n \tag{3.1}$$

where v is the velocity (cm sec^{-1}), D the diameter (cm), k a constant for a given type of snowfall having the dimensions cm sec^{-1} cm^{-n} and n an index also dependent on the type of snow. The results are shown in figures 3.2a, b; 3.3a, b; and 3.4a, b on logarithmic and linear plots and each case will be discussed below. Any given point in these diagrams represents the mean velocity within a diameter interval of 0.02 cm and has been placed in the middle of the interval. The number of measurements made is indicated beside the plotted points.

The velocity-diameter curves shown in figures 3.2a and b may be considered as typical of snowflakes (i.e. aggregates). The series of

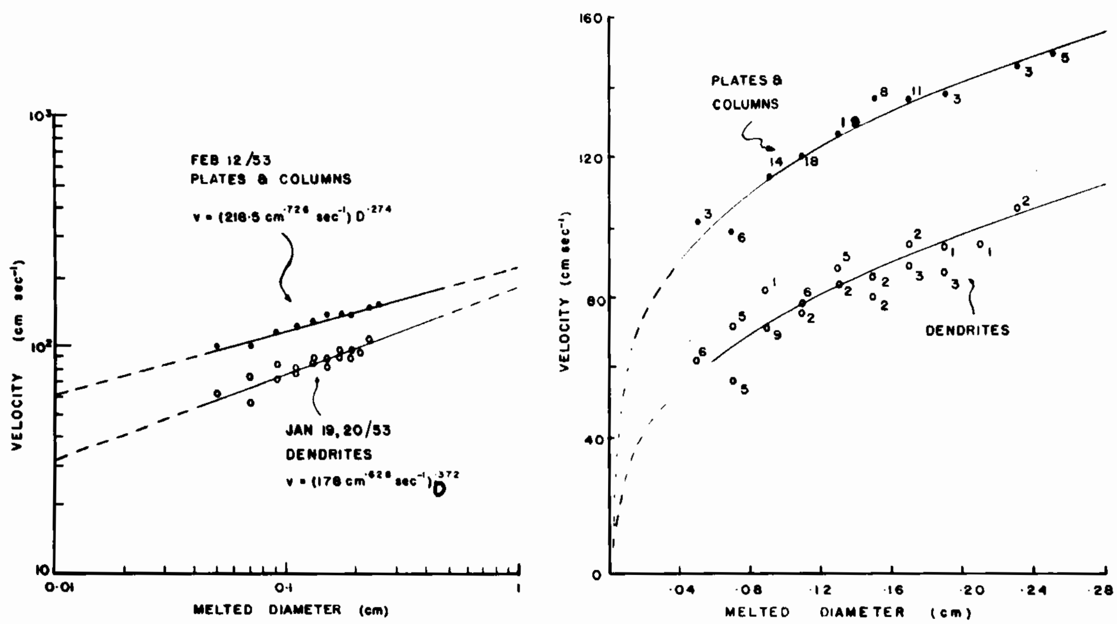

Figure 3.2a, b - Terminal velocity of snowflakes as a function of melted diameter.

points about the top curve of each diagram was obtained on 12 February 1953 from about 1100 to 1300 E.S.T. The temperature at the surface was 25F. The aggregates were found to consist of combinations of plates and columns. The points could best be fitted by using equation (3.1) where $k = 218.5\ cm^{0.726}\ sec^{-1}$ and $n = 0.274$. The bottom curves of figures 3.2 were obtained in the same manner but $k = 178\ cm^{0.628}\ sec^{-1}$ and $n = 0.372$. These curves were determined from the data obtained on 19 and 20 January 1953. The snowfall on both days consisted solely of plane and spatial dendrites, and the temperatures were 28 and 30F respectively. On a mass or melted diameter basis, it is seen that aggregates of columns and plates have a more rapid rate of descent than those made up of dendrites (the rate of fall is about 1.5 times as great). These results are quite reasonable since columns and plates are more dense than dendritic crystals. The dendrites, being feathery in appearance, have larger cross-sections than plates or columns of equal mass. The resistance offered by the air to their fall is consequently greater for dendrites than for plates and columns.

On 29 December 1952 the snowfall was made up of dendrites and of irregular assemblages of plates, and the ground temperature was 26F. The results of the measurements are given in figures 3.3a and b, the curves

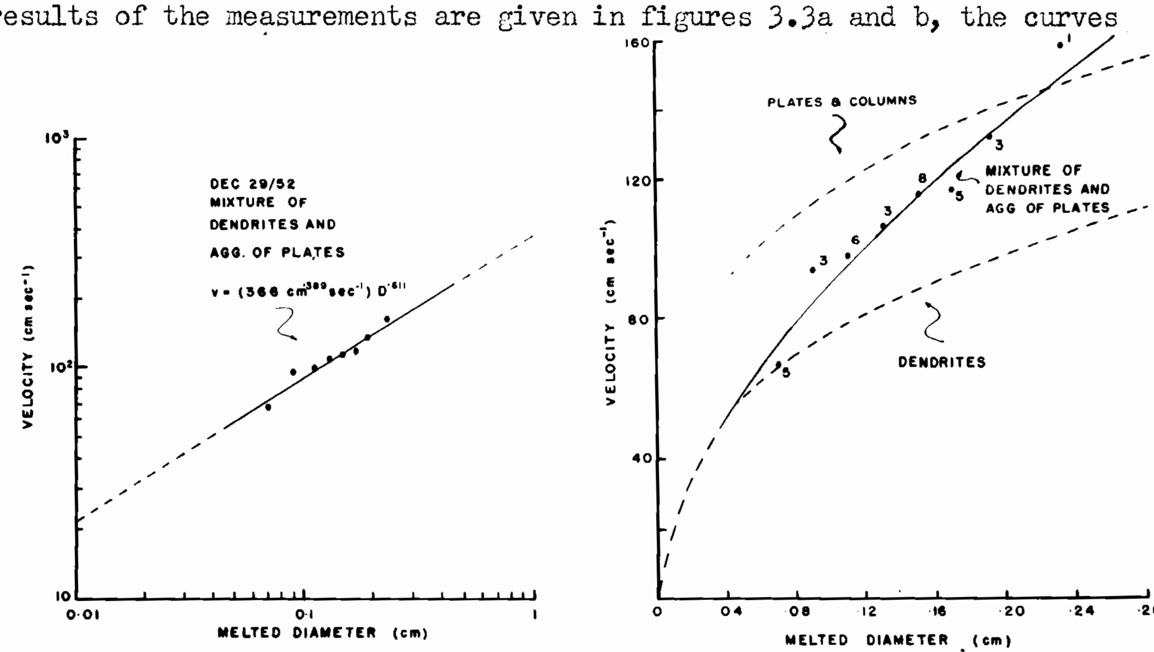

Figure 3.3a, b - Terminal velocity of snowflakes as a function of melted diameter.

of best fit having been calculated from equation (3.1) where $k = 366$ $cm^{0.389}$ sec^{-1} and $n = 0.611$. It is seen that this curve rises much more steeply than those shown in figure 3.2. (The latter are shown dotted in figure 3.3b). At the lower limit of the photographic technique used (about 0.04 cm), the velocity assumed is approximately 50 cm sec^{-1} which corresponds roughly to the velocity of dendrites of that melted diameter. The velocities increase rapidly with size and are seen to approach (and finally exceed slightly) the values of the upper dotted curve of figure 3.3b, i.e. the velocities of plates and columns. The shape of this curve may be due to one or both of the following factors. a) The dependence of the photographic method on the scattering cross-sections would heavily favour the registration of small dendritic clusters as opposed to small aggregates of plates of the same mass. This could explain why the measured velocities approach those for dendrites as the diameter decreases. b) If the main aggregation was taking place among the plates, the same phenomenon as mentioned in (a) should have been in effect. For larger diameters, however, the measured velocities should gradually approach the velocities of plates.

Finally, in figures 3.4a and b, the results have been plotted for the two remaining days. The ground temperature on 6 December 1952 was 33F so that some slight melting must have occurred. The snow was made up of very large aggregates (up to 0.36 cm melted diameter) of dendrites. The values of the parameters of equation (3.1) giving the best fit are $k = 207$ $cm^{0.678}$ sec^{-1} and $n = 0.322$. The resulting curve is seen to lie above the curve for dry dendrites which has been dotted in. Had the air been a little warmer than 33F, it is likely that the velocities would

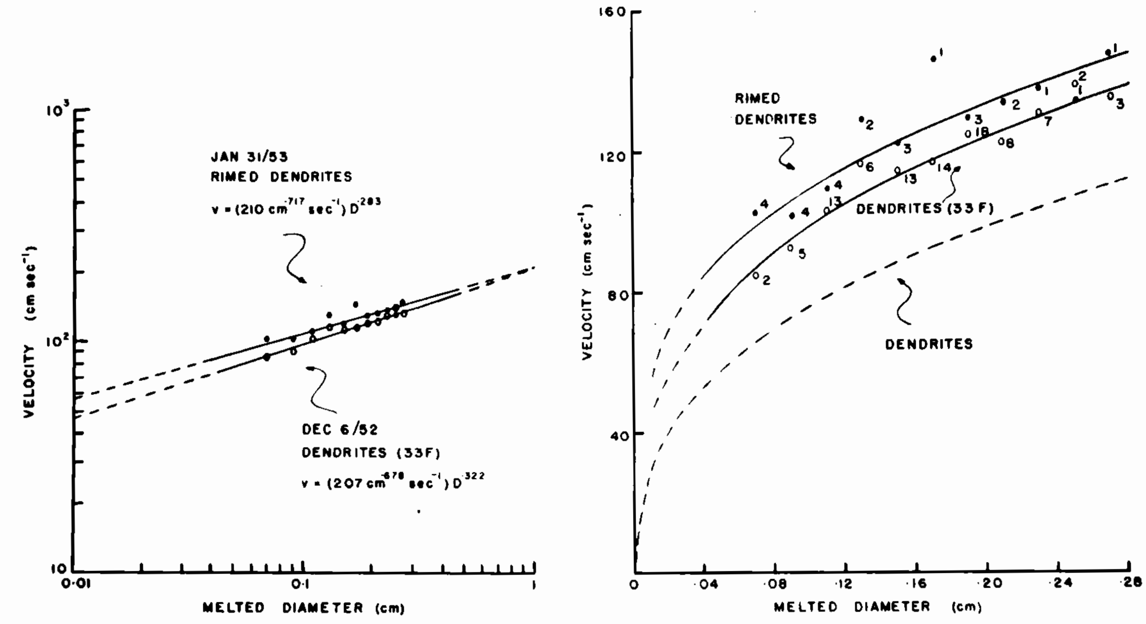

Figure 3.4a, b - Terminal velocity of snowflakes as a function of melted diameter.

then have exceeded those for plates and columns. (Preliminary measurements at the end of the winter 1951-1952 indicated that at about 35F velocities of order of 300 or 400 cm sec^{-1} are not uncommon, the precipitation still having the appearance of snow but being quite wet.) The points about the upper solid curve in figures 34a and b were obtained on 31 January 1953 from measurements of rimed snowflakes (i.e. snowflakes having numerous tiny frozen water droplets attached to them which had been picked up by coalescence in falling through a cloud layer). The aggregates consisted of rimed dendrites and plates with extensions, and the temperature was well below the freezing point, reading 25F. The k and n values of equation (3.1) that gave the curve of best fit are $k = 210\ cm^{0.717}\ sec^{-1}$ and $n = 0.283$. It is noticed that this curve has been displaced from the dendrite curve towards higher velocities due to the riming. The amount of displacement would vary from occasion to occasion depending on the degree of riming.

4. SUMMARY AND CONCLUSIONS

The velocity of fall of snow in the form of aggregates has been measured for snowflakes of equivalent melted diameter ranging from about 0.04 cm to about 0.32 cm. Tiny aggregates and single crystals were not susceptible to the technique used, but the data of Schaefer for the velocity of single crystals, though very sparse, tend to confirm our observations on aggregates.

The terminal velocity of fall of raindrops has been approximated (Spilhaus, 1948) for the purpose of radar studies by the equation $v = kD^{1/2}$ relating velocity to diameter, where $k = 1400\ cm^{1/2} sec^{-1}$. An analysis of the measurements on snow aggregates shown in figures 3.2 to 3.4 indicated that the experimental findings could be represented by $v = kD^n$ where the parameters k and n both vary with crystal type and degree of riming. The results are summarized in the first two columns of table 1.

Table 1

$v = kD^n$

Crystal Type	k $cm^{1-n}\ sec^{-1}$	n	k (for n = 0.31) $cm^{0.69}\ sec^{-1}$
Plates & Col.	218	0.274	234
Rimed Dend.	210	0.283	221
Dend. (33F)	207	0.332	203
Dend. (< 32F)	178	0.372	160
Mixed Dend. & Plates	(366)	(0.611)	--

If it is desired to reduce the parameters from two to one (for convenience in any future calculations), the data may be satisfactorily fitted by means of the same equation where, however, the index n is constant and k is the only variable parameter. The k factors for n = 0.31 are given in the third column of table 1, and curves using these parameters have been superimposed on the experimental data in figure 4.1a. The curves of figure 4.1a have been replotted on logarithmic

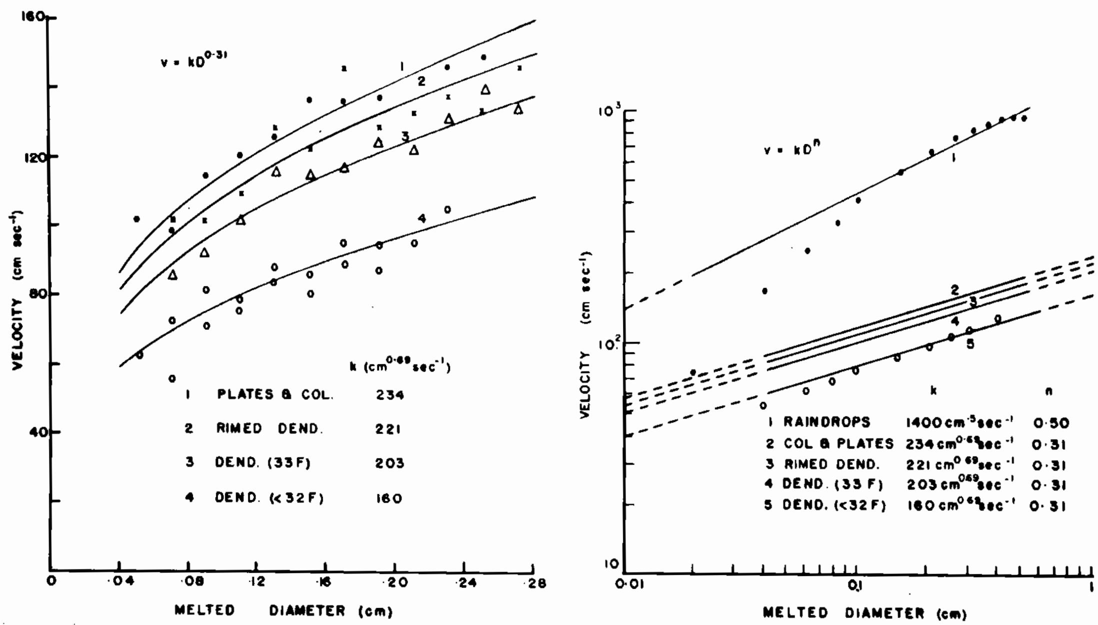

Figure 4.1a, b - Showing the goodness of fit to the experimental data of the equations $v = kD^{0.31}$

scales in figure 4.1b and are compared to the Spilhaus curve for raindrops. The points plotted about the upper curve of 4.1b represent measured raindrop velocities and have been inserted to indicate the goodness of fit of Spilhaus' relation. The series of points close to curve 5 have been obtained from the curve of best fit for dendrites from figure 3.2. The corresponding comparison using curves 2, 3 and 4 shows a much better fit. The indication then is that the divergence from measured values using our more general relationship, in which the index n is constant for a given type of snowfall, is not too serious.

An added advantage in choosing a constant index is that the parameter k then gives a measure of the velocity of fall. For instance the ratio of k (plates and columns) to k (dendrites) is about 1.5, so that the former fall 1.5 times as rapidly as do the dendrites. Of the k factors shown, the ones for dendrites and for plates and columns are the most useful. The other k values listed are typical only of the observed snowfalls since k varies with the degree of riming and also with the amount of melting if the temperature is slightly in excess of the freezing point.

The more general form of the equation (i.e. with constant n) could be easily adapted to determining size distributions in space from samples obtained by gravitational settling. Its application to radar studies of echoes from snow is also evident since the radar echo is dependent on the sum of the sixth powers of the diameters of the scatterers per unit volume of space. A more complete discussion of these problems is deferred to the radar section, Part III.

REFERENCES

Marshall, J.S., Langille, R.C. and W.McK. Palmer, 1947: Measurement of rainfall by radar. J. Meteor, 4, 186-192.

Nakaya, U. and T. Terada Jr., 1935: Simultaneous observations of the mass, falling velocity and form of individual snow crystals. J. Fac. Sci., Hokkaido Imp. Univ., Ser. 2, 1, 7, 191-200.

Schaefer, V.J., 1947: Properties of particles of snow and the electrical effects they produce in storms., Trans. Amer. Geophys. Union, 28, 4, 587-614.

Spilhaus, A.F., 1948: Drop size, intensity and radar echo of rain. J. Meteor, 5, 161-164.

PART III

SNOW PATTERNS

1. INTRODUCTION

A snow pattern frequently observed in vertical section by radar is that of oblique streaking. Marshall (1953) has interpreted this to mean that the snow is falling from persistent generating elements, the resultant sloped pattern being produced by the existing wind shear. Browne (1952) has also arrived at the same conclusion from observations on an A-scope of a fixed vertically pointing radar.

Unusually well defined patterns of this type were observed by radar at Montreal on 2 November 1951 (figure 1.1). The relation of these patterns to the wind shear has been investigated using the theory derived by Marshall and has led to a consideration of the rate of descent of the precipitation particles. It is this analysis of the data that was used in Marshall's paper.

Radar photographs, obtained during the winter 1951-1952, have been analysed to provide further information on some of the aspects of these precipitation trails and the motion of the patterns has been studied and correlated with the wind at the generating level. The rate of fall of the snow particles as a function of height has been investigated, using radar records from the winter 1952-1953, in an effort to determine regions favourable for aggregation.

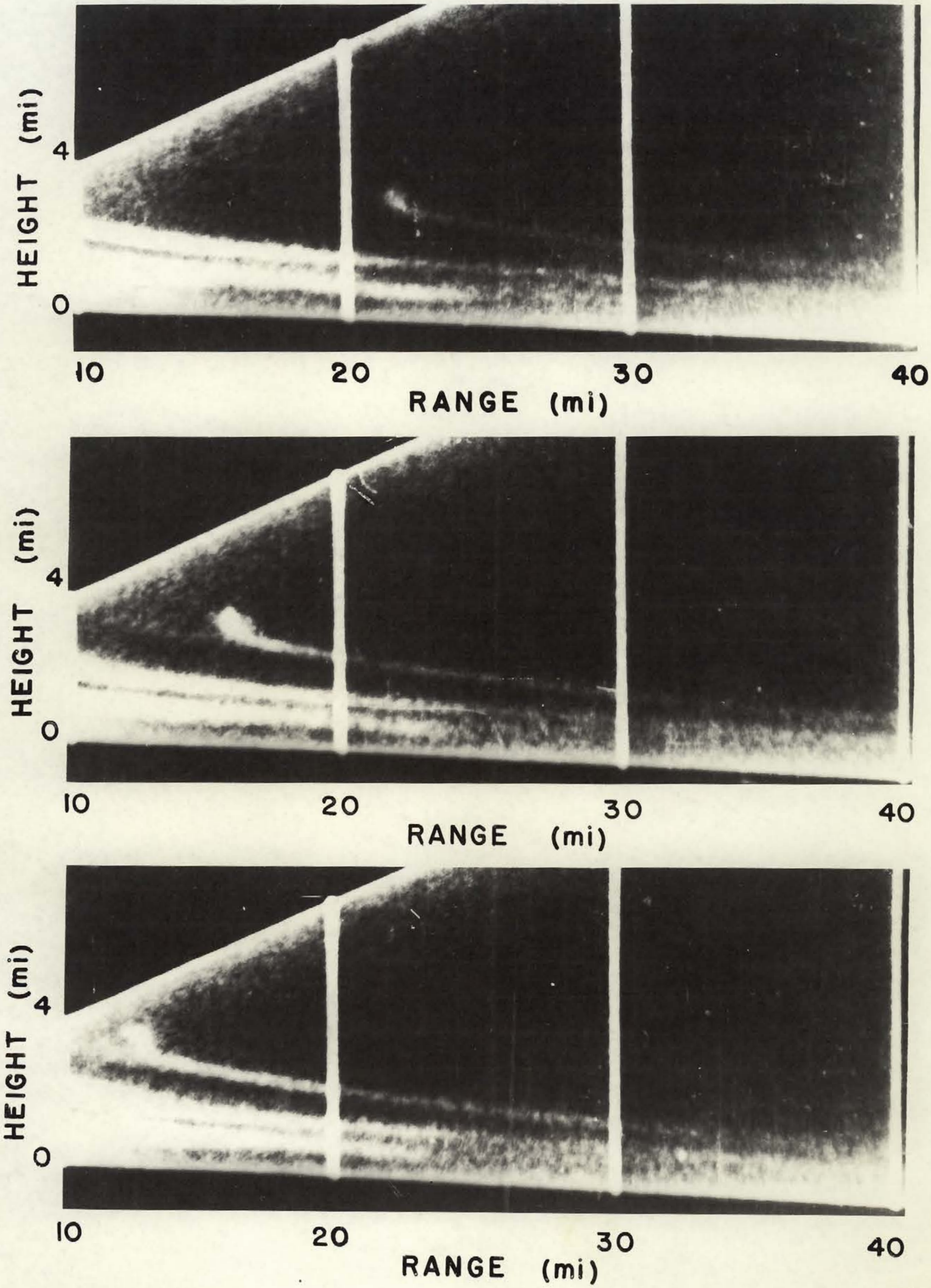

FIG.1·1 - Ten-scan exposures, 1 sec per scan, at bearing 260°, of height/range display of AN/TPS-10A radar, wavelength 3 cm, at Montreal Airport, 1600 hours, 2 November 1951.

2. THE PATTERN OF 2 NOVEMBER 1951

According to Marshall, the equation of the trajectory formed by a particle in falling through a wind shear is given by

$$x - x_o = \int_o^z \frac{w(z)}{v(z)} \, dz \tag{2.1}$$

where x measures horizontal distance from the initial point x_o,

z is the vertical distance measured downward,

$w(z)$ is the wind component in the direction of x at depth z,

and $v(z)$ is the velocity of fall of the particle.

If a generating cell, which emits particles all having the same rate of fall, is considered to move with the wind W at $z = 0$, the pattern formed by the precipitation trail coincides with the trajectory of the particles when referred to axes moving with the generating element. The slope of the pattern with reference to these same axes is

$$\frac{dz}{dx} = \frac{v(z)}{w(z)}, \tag{2.2}$$

from which the rate of fall of the particles can be determined in terms of the wind profile. The pattern as a whole moves with horizontal velocity W, the wind at the generating level with respect to the ground. The height of the pattern directly over a fixed point on the earth's surface then changes continuously as the pattern passes overhead. The apparent rate of descent of the pattern, referred to a fixed point on the earth, is given by $W \frac{dz}{dx}$ and thus varies with the slope.

A special case of equation (2.1) results when the rate of fall of the particles and the wind shear are both constant with height. The pattern in space is then parabolic in shape with the vertex at the generating level.

2.1 Application of the Marshall Theory

A series of clearly defined snow trails was observed by radar* on 2 November 1951. The generating cells were at an altitude of 15000 ft and were spaced roughly 20 miles apart. The patterns moved towards the radar approximately from the west at a speed of 90 mi hr^{-1} which was found to correspond to the westerly wind at 15000 ft. The pattern of this particular day, and so the radar photographs, was far superior to any others of the winter 1951-52. This pattern was then the most amenable to measurement and interpretation.

Since the wind profile along a bearing of 260° (the radar bearing) was found to increase almost linearly with height, theoretical semi-parabolic patterns have been drawn in the lower part of figure 2.1 and the theoretical slopes, rate of descent of the pattern relative to a fixed point on the earth, and rate of fall of the snow particles are given in the upper part of the diagram.

The photographs of the range/height indicator (see figure 1.1) were analysed and the results are shown in figure 2.1. Pattern data pertaining to six trails, as obtained from radar photographs at bearing 260 or 80° and from the wind shear, have been superimposed on the theoretical curves given.

The slope of the pattern was determined from the radar pictures, not without some difficulty. The distortion in the radar display tended to be as great as the measured slopes and so a careful calibration of the range/height indicator had to be made. (This is discussed in full

* Radar specifications: wave length 3.2 cm, peak power 65 kw, pulse length 1 μsec, p.r.f. 1000 sec^{-1}, beam 2° horizontal X 0.7° vertical, polarization vertical.

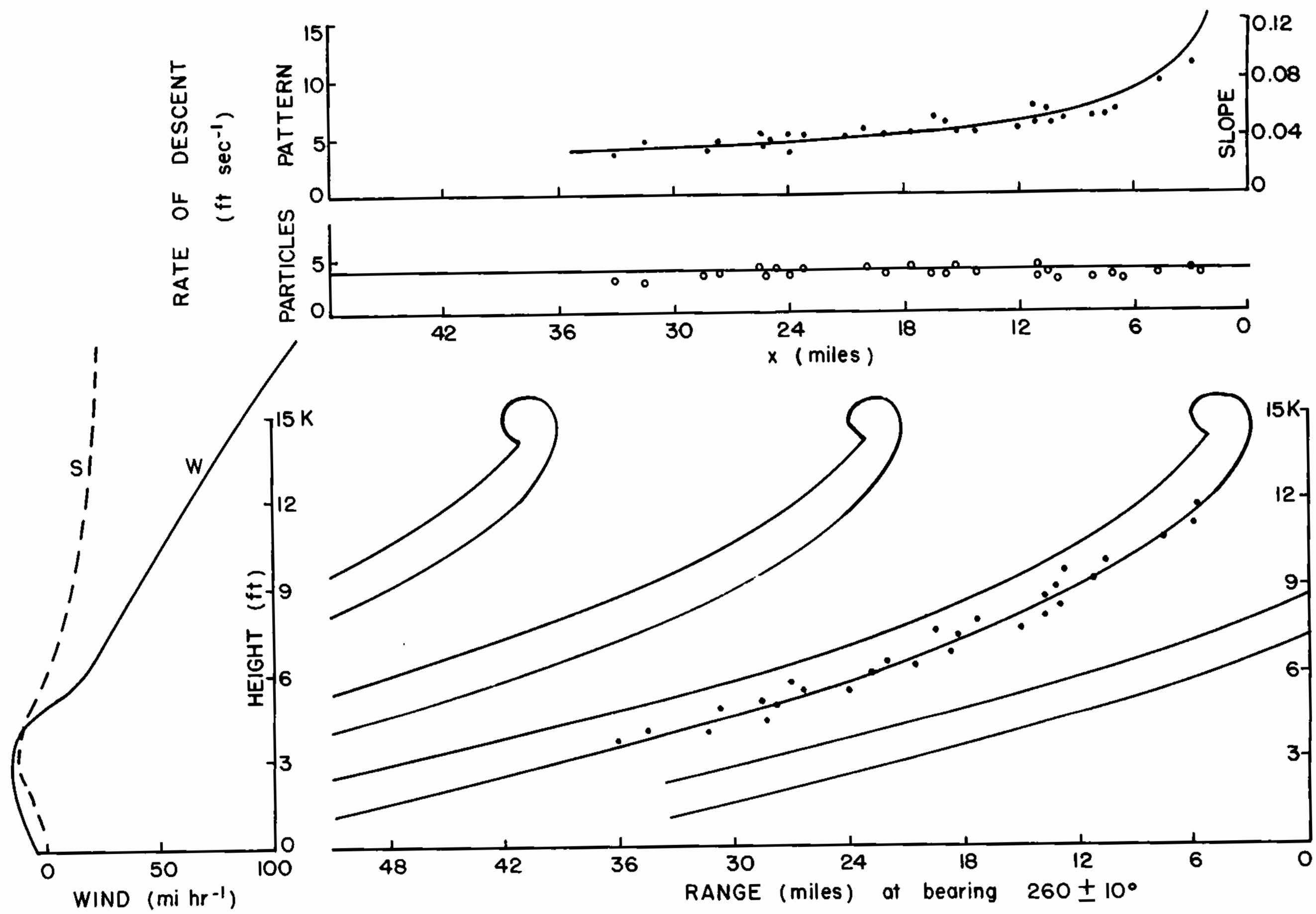

Figure 2.1 - Height/range data from six trails such as shown in figure 1.1 are plotted in the main diagram, and fitted by a parabola. These are combined with the winds to give rate of descent of the particles (open circles). The measured slopes of the trails at various horizontal distances back from the generating elements are shown at the top, with an alternate scale of rate of descent of the pattern.

detail in the appendix.) The measured slopes are seen to fit the theoretical curve quite well. The slopes decrease rapidly with increasing distance from the vertex of the parabola, soon becoming very small. The alternate scale of rate of descent of the pattern in the upper portion of figure 2.1 has been obtained from a combination of the slopes with the wind at the generating level. The rate of fall of the snow particles (actually the rate of fall of maximum signal intensity) as calculated from equation 2.2 was found to be 4 ft sec^{-1} independent of height as is shown in figure 2.1. Measured heights as a function of distance from the apex of the pattern are compared to semi-parabolas in the bottom part of the diagram.

This analysis and the appendix represent the author's contributions to the joint report of Marshall, Langleben and Rigby (1952).

3. FURTHER ANALYSIS OF RADAR RECORDS

The clearly defined parabolic patterns observed on 2 November 1951, which appeared almost periodic are not common occurrences. Most of the photographs obtained during the winter 1951-1952 showed the same sort of pattern, none of them, however, being as well defined. These records have been analysed to provide further evidence of the validity of Marshall's theory of precipitation trails formed by falling snow. Since the RHI display (figure 1.1) is particularly suited for following the motion of a pattern, it was possible to investigate the horizontal velocities of these patterns and relate them to upper air winds.

During the winter 1952-1953, a zenith pointing, 3 cm, radar was used. The film record obtained, discussed in greater detail in section 3.2, was a continuous recording of the height of the echo in the vertical against the time of observation. This mode of presentation had the advantage that the height scale was undistorted as compared to the troublesome distortion of the RHI display used in the earlier analysis. The slopes of the precipitation trails were then easily measured and, when combined with upper wind data, were used to investigate the velocity of fall of the snow as a function of height.

3.1 Winter 1951-1952: AN/TPS-10A

In section 2, it was postulated (and verified for the case of 2 November 1951) that the generating cell moved with the wind speed at its own height. This postulate is now given further verification by comparing measured velocities of the generating elements with the wind velocities. (The wind profiles were obtained from radio-sonde observations and upper air charts analysed by Mr. B.A. Power. The closest available radio-sonde station was at Rome N.Y. When no data was available from Rome, extrapolations were made from ascents at Buffalo N.Y. and Portland, Me.)

In the following analysis, use is made of the terms "echo height" and "velocity height". The former is the height of the top of the echo as measured on the radar records, being the height of the top of the generating cells when visible or the maximum echo height when no cell was detected by the radar. The velocity height is obtained by finding the height at which the wind has the same velocity as that measured for the generating element. When no generating cell is visible, the velocity of any part of the trail can be used to find the generating level since the pattern as a whole moves with the same horizontal speed.

Since the radar bearing was generally not along the wind direction at the generating level, several assumptions must be made about the generating cells. It is assumed that a cell is of fair horizontal extent and that its leading edge is perpendicular to the wind direction (figure 3.1). Under these conditions, the velocity v_R, as obtained from the radar is related to the true velocity, v_W by

$$v_R = v_W \sec \theta$$

where θ is the angle between the radar bearing and the direction of motion of the generating cell. On a polar diagram, the intersection of a circle whose diameter is the vector v_R with the wind profile (figure 3.1, right) leads to a value of v_W and of θ. Occasionally, the wind profile may closely follow the circle over a considerable range of heights, in which case a height determination is possible only if radar observations have been made along two different aximuths.

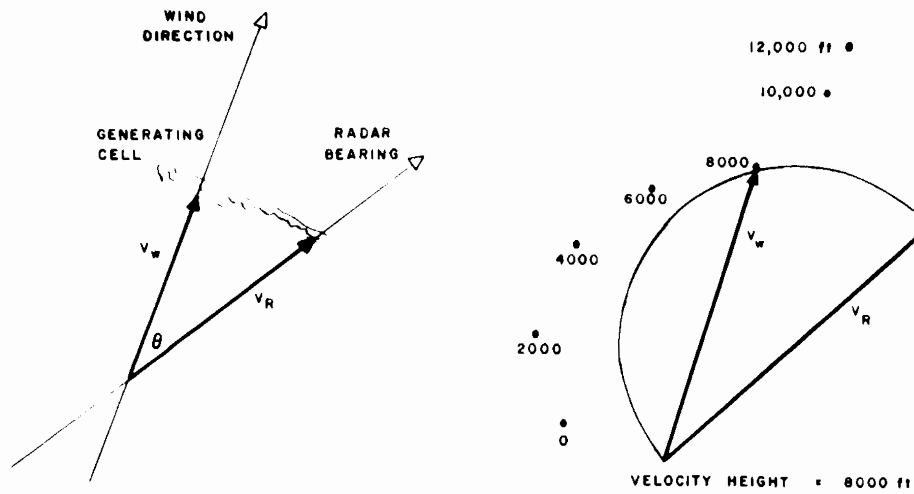

Figure 3.1 - The diagram at the left relates the horizontal velocity of the generating cell to its velocity as measured along the radar bearing. The method of obtaining the velocity height is shown at the right, where a circle of diameter v_R intersects the wind profile on a polar plot.

Also the upper air wind data are such that, at best, the uncertainty in a velocity height is about 1000 ft.

Radar photographs of precipitation patterns were obtained on nineteen separate occasions (Gunn, Langleben, Dennis and Power, 1953) during the winter of 1951-1952. Of these, sixteen contained sufficient radar information to determine radar velocities. Generating cells were detected on ten of these sixteen days and the velocity heights for theses cases were in excellent agreement with the observed echo heights, the mean echo height being some 600 ft above the mean velocity height (figure 3.2): the correlation coefficient between the two was 0.96. Since the average cell depth was of the order of several thousand feet, it is seen that the cell moves with the air speed quite close to its top. No cells were visible on four of the sixteen days. For these cases it was found that the pattern moved

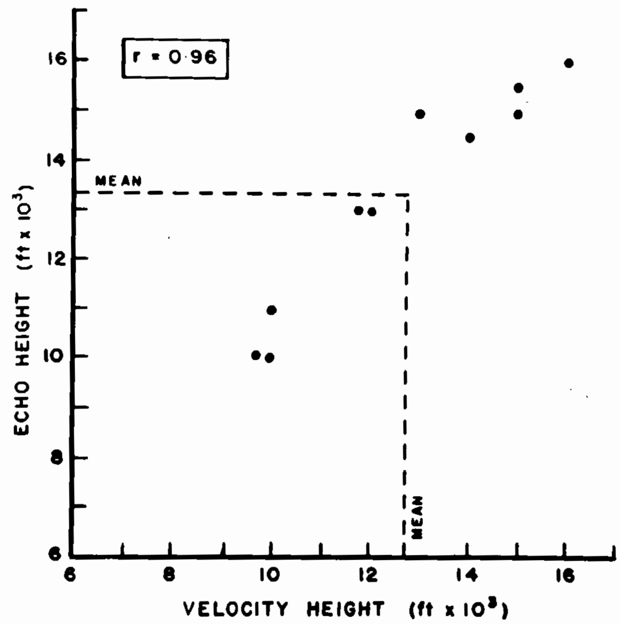

Figure 3.2 - A scatter diagram showing the correlation between echo height and velocity height for the ten cases in which the generating elements were observed.

with a velocity equal to that of the wind about 1100 ft above the top of the echo. On this basis, it seems justified to assume that the generating cell did exist some 1000 ft above the echo top, the radar sensitivity being too low to detect the actual cells. The remaining two days of pattern had wind profiles which made velocity height determinations unreliable, and the velocity of the trail was equal to that of the wind about 6000 ft below the echo top.

Considering the possible errors inherent in the methods used for obtaining the wind profiles and in the measurement of height, it is remarkable that such close agreement should exist between echo height and velocity height. This is surely a confirmation of the thesis that the generating elements do in fact usually move with the air at their own levels.

3.2 Winter 1952-1953: Zenith Pointing Radar

A zenith pointing radar* was installed during the summer of 1952 and was in operation by the fall. The method of recording the radar display was as follows. The received signal was used to intensity modulate a stationary trace on an oscilloscope. A camera was constructed (with the help of Dr. Gunn and Mr. G. Tweeddale) in which continuous motion of a film was achieved by means of a driving mechanism whose speed was variable. The direction of motion was perpendicular to the trace on the scope and the resulting display on the film was of height against time. This method has the advantage that the display is a perfect rectangular grid as opposed to the distortion of the AN/TPS-10A. Lines of constant height are parallel to the base line and equally spaced for equal height intervals. Time intervals are known from the rate of motion of the film and the time axis is at right angles to the height axis.

Suppose that a precipitation trail, of the kind being discussed, is carried by the wind through the beam of the radar. Initially, the leading edge or generating cell is recorded on the film. At some later time, another part of the trail is passing through the radar beam, but the film has moved on through the same time interval and the echo overhead is recorded at this later time. Thus the complete precipitation pattern in space is reproduced on the film.

Because of the simplicity of this display it was thought desirable to amplify the findings of 2 November 1951 on the vertical velocity component (or terminal velocity) of snow particles. For this an accurate knowledge of the wind profile was also required, since the velocity of fall is given by

* Radar specifications: wave length 3.2 cm, peak power 40 kw, pulse length 0.75 μsec, p.r.f. 500 sec^{-1}, beam 2°.

$v(z) = \frac{dz}{dt} \frac{w(z)}{W}$, where the symbols have the same meaning as in section 2. The remarkable agreement between echo height and velocity height in section 3.1 indicated that Mr. Power's analysis was rather more reliable than he had expected, and was sufficient justification for placing fair confidence in any subsequent data obtained in similar fashion.

Three days of good pattern were picked from the radar records obtained for the winter 1952-53. A complete analysis of all the available film would have been very lengthy, and it was felt that the data obtained from a few films would furnish the information required. A sample picture of the display is shown in figure 3.3. The results for the three days are given in table 1, which also includes other relevant data such as crystal types observed at the ground, the height and the temperature of the generation level, and the wind direction at that level. Wind components at lower levels have been taken along this same aximuth.

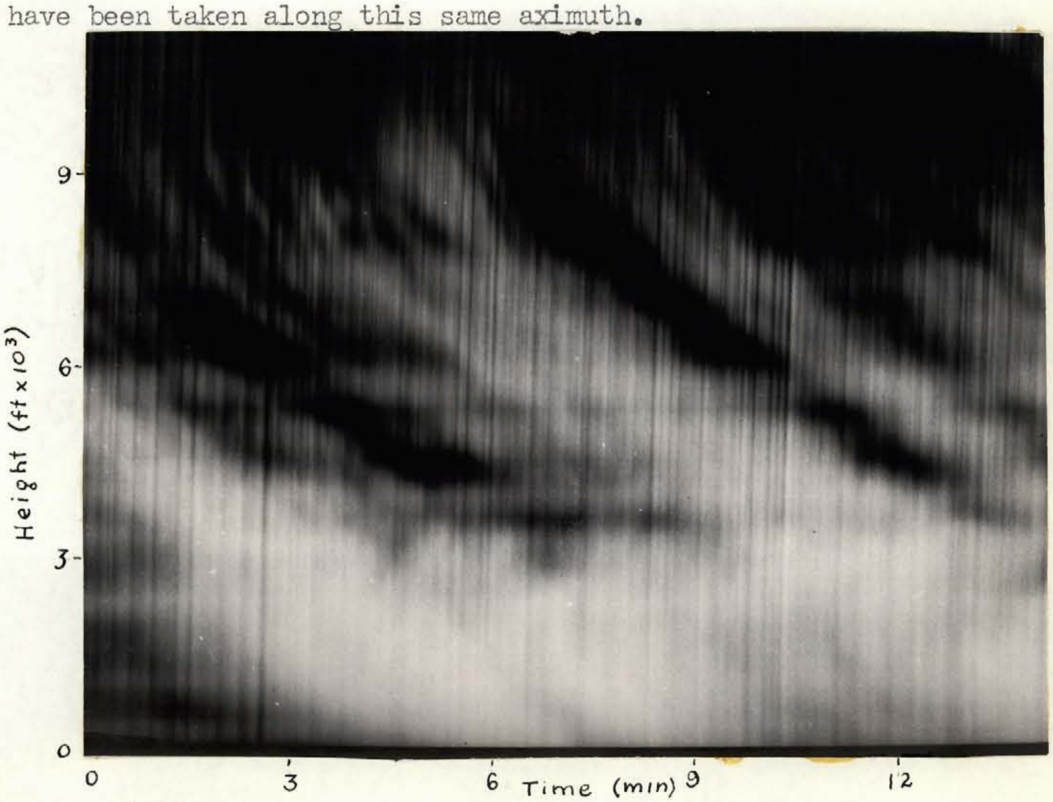

Figure 3.3 - A typical snow storm pattern recorded by the zenith pointing radar.

Table 1

Height ft	Wind knots		$v(z)$ ft $\sec^{-1}$	Dev'n from mean	Remarks
11,200	48		g.ℓ.*		13 Jan. 1953: 1015 hours
9200	41		2.94	0.05	Wind components along 280°
7200	38		2.85	-0.04	Generating level at 11,200 ft, -10.5C. Crystal types:
5200	31.5		3.00	0.11	i.a.c.p.**, capped col., plates, very little
3200	23		2.77	-0.12	aggregation
		mean	2.89	0.08	
12,000	60		g.ℓ.		28 Jan. 1953: 1015 hours
10,000	50		3.37	-0.04	Wind components along 220°
8,000	39.4		3.96	0.55	Generating level at 12,000 ft, -14C. Crystal types:
6,000	34.5		3.19	-0.22	needles, p.w.s.e.***, some aggregation
4,000	28.5		3.13	-0.28	
		mean	3.41	0.27	
15,500	48.25		g.ℓ.		2 Feb. 1953: 1700 hours
14,000	44		3.30	-0.16	Wind components along 260°
12,000	38		3.56	0.10	Generating level at 15500 ft, -21C, Crystal types:
10,000	33		3.38	-0.08	plane and spatial dendrites, p.w.s.e, very large
8,000	18		(4.48)****		aggregates
6,000	15		3.58	0.12	
		mean	3.46	0.12	

---

* g.ℓ. - generating level

** i.a.c.p. - irregular assemblage of columns and plates

*** p.w.s.e. - plates with simple extensions

**** This high value is thought to be due to an error in the winds. The upper air charts indicated the presence of a secondary front at 8000 ft with a consequent sudden change in wind speed and direction through this frontal zone. An error of 500 ft in the estimation of the frontal height would bring the measured velocity of fall into line with the others.

Several conclusions can be drawn from the data of table 1. It is at once apparent that the velocity of fall of the snow particles as determined from the radar echo was reasonably constant with height on any given day. Also, these velocities were of the order of 2 or 3 times greater than the velocity of fall of individual snow crystals (average about 1.5 ft sec^{-1}) as measured by Schaefer and Nakaya and Terada (Part II). The significance of these facts will be considered further in the next section.

The velocity of fall of the snow particles as discussed here is not to be confused with the rate of descent of the pattern overhead as observed by the radar at the ground. Taking the first case of table 1 as an example, the rate of descent of the pattern decreased from 20.2 ft sec^{-1} when the echo was at 9200 ft to 5.3 ft sec^{-1} when the echo height was 3200 ft.

4. SIZE DISTRIBUTION AND VELOCITY OF FALL

The theory of section 2 assumed that the generating element was emitting particles having all the same velocity (i.e. that a monodisperse distribution existed at the generating level). It has been thought that snow fell for considerable distance as individual crystals before aggregation commenced. Our radar studies indicate that when the snow is formed in compact cells, its velocity of fall quite close to the generating level (i.e. before any significant change in size distribution has taken place) may be several times the velocities associated with single crystals and of the right order of magnitude for snow aggregates. There is then reason to believe that on these occasions sufficient turbulence and updraft may exist in the formation region to promote effective aggregation of the snow crystals, and yield a wide distribution.

Starting with such a distribution at the generating level and assuming that no break up or further aggregation takes place, there would be a sorting of the snowflakes according to size with distance fallen since each size, having its own velocity, would trace out a different trajectory, the resulting pattern in space broadening out as the distance of fall through the wind shear increased. On the other hand, if aggregates break up and the new ones form throughout the fall, the average size distribution will remain the same, and the pattern will not broaden. Virtually nothing is known about aggregate size distributions in space and their modification with distance and, in all likelihood, a combination of the above effects is at work.

4.1 Velocity of Fall from Radar Echo

The intensity of the signal back-scattered from many incoherent scatterers, as for example from precipitation in any form, is proportional to $N_D D^6$, where N_D is the number of particles of diameter D and the summation has been taken for a unit volume of space. The radar sensitivity is such that only a limited region about the peak of the $N_D D^6$ versus D curve (figure 4.1) contributes to the observed echo. In a wide distribution, the small scatterers, though very numerous, make

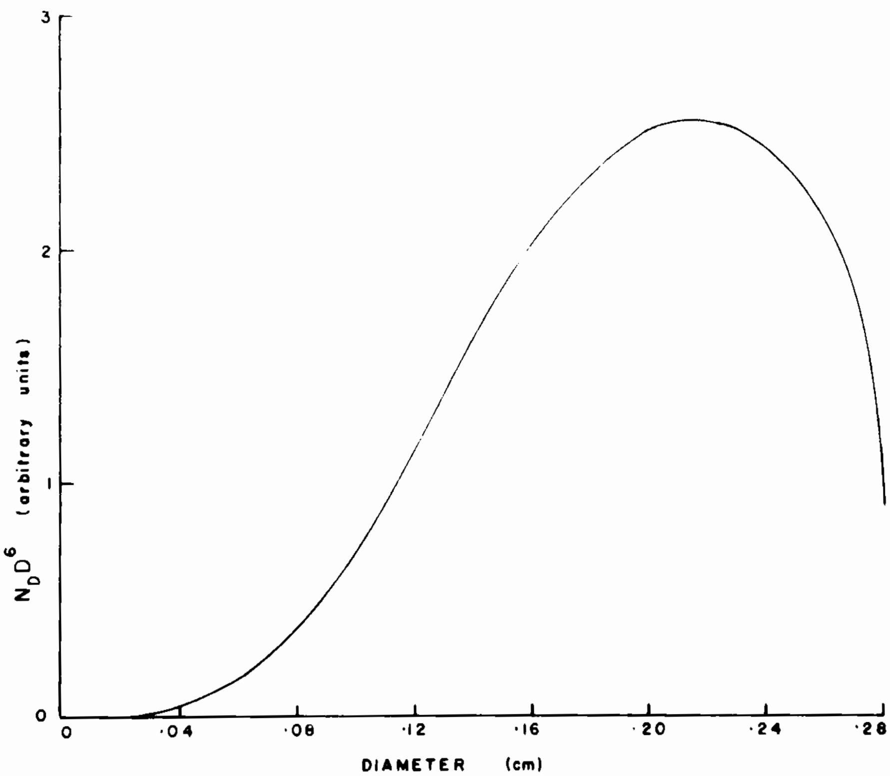

Figure 4.1 - A typical snow distribution due to gravitational settling has been combined with a velocity curve to yield the size distribution in space and then converted to give a measure of the contribution to the radar echo as a function of particle size.

insignificant contribution to the echo as compared to the larger scatterers. The radar echo from the precipitation trails thus represents the peak of the $N_D D^6$ distributions at all heights.

Now we have shown that the rate of fall of the snow (as determined from the maximum intensity of the radar echo) was invariant with height. The most obvious, but not necessarily true conclusion, is that the size distribution does not change with height. Another possibility is that since the larger particles of the distribution, whose velocities vary in the significant region by less than a factor of 2 (as opposed to 9 in rain), are of importance radarwise, the size distribution is but slightly modified with height, tending to give the same results. It is also apparent that snow does not aggregate gradually during its course of fall on occasions when it is formed in compact cells. For if it did, the velocities measured from the radar pictures would gradually increase with distance fallen.

5. CONCLUSIONS

The theory of Marshall on snow precipitation trails has been substantiated using radar records of two winters. The height of the generating cells as measured on the radar display was compared to the height at which the upper air winds had the same velocity as the cell, and the correlation coefficient between the echo height and velocity height was 0.96. It may thus be said that the generating elements move horizontally with the wind speed at about their own level.

The radar analysis has also yielded the fact that snow does not aggregate gradually during its course of fall, but that the aggregation is perhaps occurring at the generating level, since the velocities measured near that level are comparable to aggregate velocities (Part II). It has also been shown from radar measurements of the rate of fall of the snow that the peak of the distributions of $N_D D^6$ versus D does not change significantly with height. For the purpose of future radar studies, and until actual measurements of size distributions in space are made for snow at all heights, it is suggested that the distribution be assumed constant with height. (Transients at the beginning and end of the storms should be excepted.) A measurement of the distribution due to gravitational settling at the earth's surface when combined with the velocity curves of Part II would then yield the distribution in space.

It is also worth remarking as seen in table 1 of section 3.2 that the air temperature within a generating element will in general identify the crystal type. Thus the water cloud in the formation region must be quite dense with some degree of supersaturation with respect to water existing. If that were not so, as for instance in the ice clouds formed at high altitudes, a knowledge of the actual vapour density excess of the ambient vapour density over that close to the ice crystal would still be necessary for crystal type determinations as was implied in Part I.

APPENDIX

Calibration of the Range Height Indicator of the AN/TPS-10A Radar

A careful analysis of the photographic records of the AN/TPS-10A RHI display taken on 2 November 1951 threw suspicion on the accuracy of the range/height calibration and led to a more thorough investigation of the calibrating process. As a result several problems arose which will be discussed here.

On that day a series of generating elements followed by long snow trails was visible on the RHI approaching from the west and then passing eastward. It was noted that the apparent altitude of a particular cell decreased as the echo approached and then increased after the echo had passed overhead and was receding. This seemed to be a very unusual property for the cells to possess. Another curious feature was discovered when attempts were made to measure the slopes of the precipitation trails from the radar photographs. With the radar antenna pointing to the east, the measured slopes at some given height appeared to be of much greater magnitude than when the set was oriented to the west.

A1. Primary Calibration and Possible Errors

For reasons already mentioned, it was thought desirable to make a careful check of the calibrating process. In normal operation, the antenna oscillates in elevation from -2^{o} to $+23^{o}$ once a second and may be swung in azimuth through 360^{o}. To calibrate, the antenna is stopped and clamped at various angles of elevation within the 25° interval corresponding to numbered settings given on a clinometer. At each angular setting a trace is registered on the radar scope with a series of dots superimposed on it at 10 mile intervals out to a range of 60 miles.

These traces are registered on photographic film. An enlarged drawing of the display is shown in figure A1. The numbers to the right of the figure, serving to identify the traces, are related to range/height data given by the makers. Thus 1 represents the horizontal; 13 denotes a height of 10,000 feet at a range of 10 miles, etc. A list of these basic data is given in table A1. It is however necessary to obtain

Table A1

Trace no. 0	-----	base of display	
1	-----	horizontal	
2	-----	10,000 feet at	60 miles
4	-----	10,000	50
5	-----	10,000	40
6	-----	10,000	30
8	-----	10,000	20
9	-----	35,000	60
10	-----	20,000	30
11	-----	25,000	30
13	-----	10,000	10
14	-----	35,000	30
15	-----	40,000	30
		top of display	

more such reference points before lines of constant altitude can be drawn. This is done by recalling that a given trace represents the beam being sent out at a certain angle. Thus trace 5, for example, which denotes a height of 10,000 feet at 40 miles, will also represent 5,000 feet at

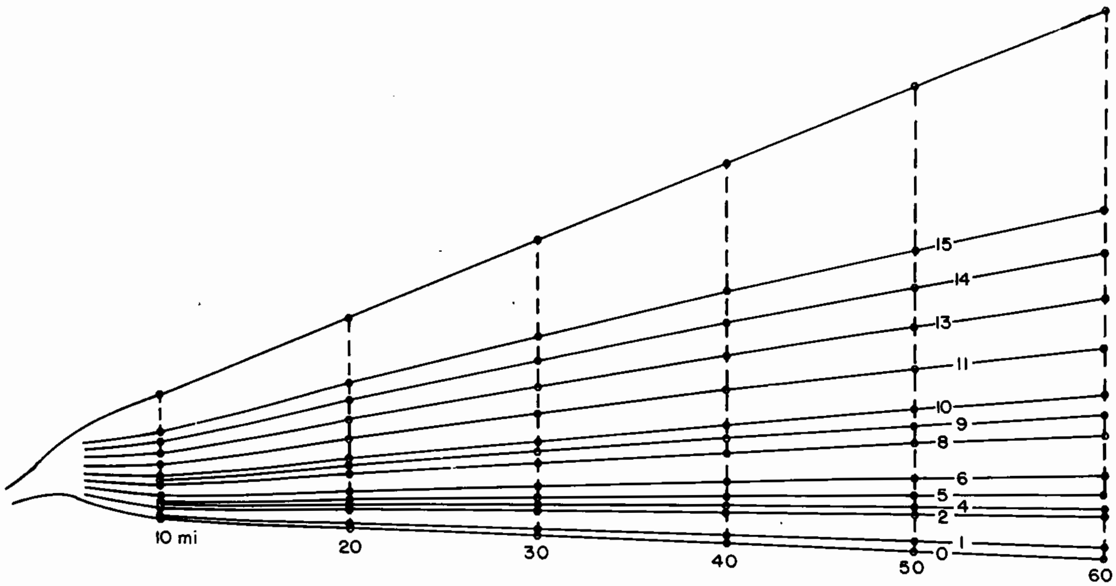

FIG. A1 - Tracing of the AN/TPS-10A display of the Range Height Indicator when the antenna is clamped at the various angles of elevation used for calibration.

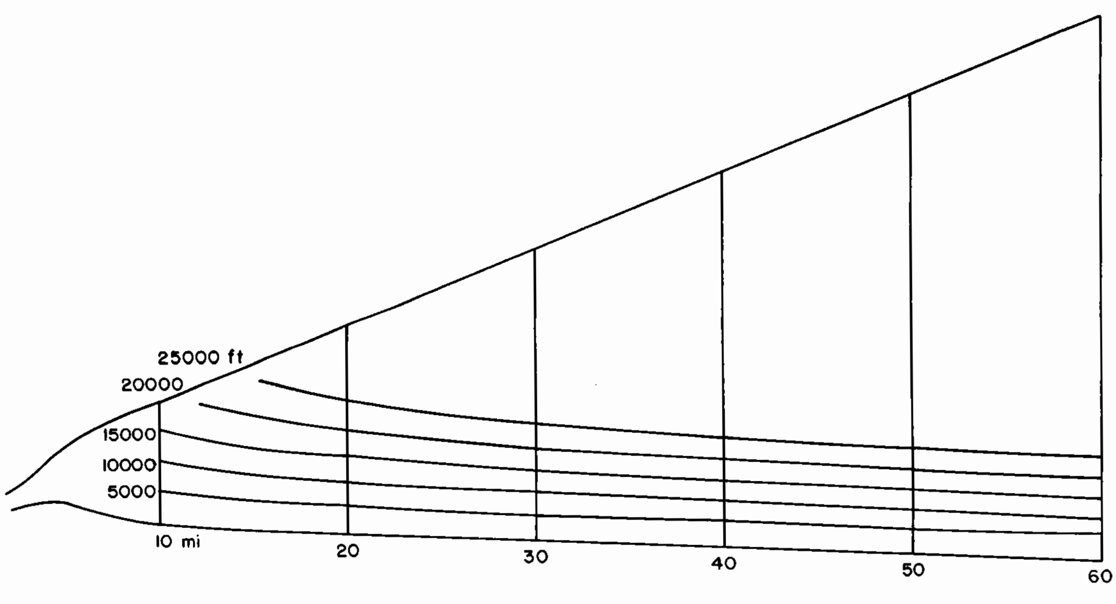

FIG. A2 - Outline of RHI display showing the calibration as contours of constant height.

20 miles. In this manner loci of constant height may be drawn. The resultant range/height calibration is as shown in figure A2.

For this calibration to apply at all azimuths, the antenna mount must be properly levelled, the 25^{o} elevation scan must be between the proper limits of -2^{o} to $+23^{o}$, and the beam should be normal to the reflector. Faults in any of these may cause serious error in determination of heights. It is possible to distinguish between, and so correct for, the errors which may arise from these sources. If the antenna mount has not been correctly levelled, the apparent height of an object as seen on the RHI depends on its bearing from the radar. The echo will appear to be high where the tilt is downward; low at 180^{o} to that direction; and at its true altitude when viewed at right angles to the former bearings. If, on the other hand, the antenna mount is level but either of the other two possible faults are present, the resulting error in altitude is independent of azimuth and depends only on the range of the echo from the radar.

A2. Methods of Checking the Calibration of the Display

a) Balancing Sections at Opposite Azimuths: The type and magnitude of the error present was determined by analysing the photographic records of 2 November 1951. When measuring slopes of the precipitation patterns, it was found that the slopes, when the patterns were to the east, were much greater than when they are viewed at the opposite azimuth. By averaging the slopes at different heights it was possible to obtain results consistent with the theory of section 2. The slopes were in error by an amount 0.024 corresponding to an angle of tilt of 1.25^{o}.

It has already been mentioned that the apparent height of the generating cells appeared to vary with range, the altitude increasing with range independent of azimuth. After applying the above correction factor, the generating cells were found to move at constant altitude. Thus it became apparent that the radar antenna was either not scanning in elevation between the proper limits or that the radiating horn was off the focal point of the reflector.

b) Bright Band: Errors in alignment of the antenna may be detected from measurements on the height of bright band. This was done on several occasions during the winter 1951-52 when a good bright band was present. A few of the analysed records are presented in table A2. It is seen that the resultant heights, based on a correction of 1.25°, were constant with range at any given time.

Table A2

	Range miles	Apparent Height feet	Correction to Height feet	Real Height feet
No.1	10	6,200 ± 500	1,100	5,100
at	20	7,400	2,250	5,150
200°	25	8,000	2,800	5,200
No.2	10	6,500 ± 500	1,100	5,400
at	20	7,800	2,250	5,550
330°	30	9,000	3,370	5,630
No.3	15	11,800 ± 500	1,750	10,050
at	20	12,300	2,250	10,050
230°	25	12,900	2,800	10,100

c) Aircraft: Accuracy of calibration may be checked by using aircraft. An aircraft flying at constant altitude over the radar at any bearing and then at 90° to that direction provides sufficient information to correct any errors in calibration. A test of this kind could not be arranged until April, 1952. The same error was still present, indicating that the display had not changed appreciably during the course of several months.

A3. Method of Determination of Heights and Slopes of Precipitation Trails

True heights were obtained by superimposing the echo on the range/height calibration grid, reading off the apparent height and correcting for the 1.25° tilt. The correction was made by reducing the apparent height by an amount which varied only with range. It was somewhat more difficult to measure the slopes of the precipitation trails because of the distortion of the grid. Also, as there was a strong wind shear present, the patterns rapidly approached the horizontal and true slopes of the order of 3 or 4 in a 100 were quite common (figure 2.1).

The method of obtaining the true slopes of a precipitation pattern can best be explained by citing an illustration. The slope of the pattern, at any height, was determined by measurement, and from it was subtracted the slope of the constant height line (figure A2). This would normally yield the correct slope but, because of error in alignment of the antenna, a further slope equivalent to 1.25° had to be subtracted. The following are values typical of those found on 2 November 1951. When the radar was bearing west, the apparent slope of the pattern at a true altitude of 8,500 feet and range 15 miles was -0.128; that of the constant height line -0.092 at that point; that of the correction factor 0.024. The correct slope was therefore -0.128 + 0.092 - 0.024 = -0.060. After the pattern had moved 30 miles eastward, the same point of the pattern was still at 8,500 feet altitude, but 15 miles to the east. The true slope was now equal but opposite in sign to the former case, being made up of the corresponding slopes -0.008 + 0.092 - 0.024 = 0.060.

References

Browne, I.C., 1952: Precipitation streaks as a cause of radar upper bands. Quart. J. Roy. Met. Soc., 78, 338, 590-595.

Gunn, K.L.S., M.P. Langleben, A.S. Dennis and B.A. Power, 1953: Radar evidence of a generating level for snow. "Stormy Weather" Research Group, Scientific Report MW-13 under U.S.A.F. Contract No. AF 19(122)-217. Also submitted for publication to J. Meteor.

Marshall, J.S., 1953: Precipitation trajectories and patterns. J. Meteor, 10, 25-29.

Marshall, J.S., M.P. Langleben and E. Caroline Rigby, 1952: Precipitation trajectories and patterns. "Stormy Weather" Research Group, Scientific Report MW-8 under U.S.A.F. Contract No. AF 19(122)-217.

PART IV

REVIEW

REVIEW

The diversity of crystal forms observed in natural snow (and their beauty) has been the object of much interest and conjecture to keen observers for many centuries. Most of the studies, however, have until recently been very qualitative. At present, snow crystal growth and its consequent fall can be described in some detail.

The success of Nakaya's group in growing snow crystals in the laboratory, as illustrated by their time lapse microphotographs, has indicated that the type of snow crystal growth is dependent on the meteorological conditions in the vicinity of the growing crystals. Now the equilibrium vapour density over water is greater than that over ice at the same temperature, so that, for example, in a water saturated atmosphere, a gradient exists which transfers vapour to the ice crystal where it sublimes. Our studies show that snow crystal growth requires an ambient vapour density which considerably exceeds that at equilibrium with the ice crystal. The interpretation of the Nakaya experiment had led to a theory of snow crystal habit in which the basic assumption is that the surface vapour density varies over the crystal surface depending on the curvature. Crystal type is determined principally by the difference between the ambient vapour density and the equilibrium vapour density at the ice crystal temperature. The mode of development of the crystal then depends on the ability of this vapour density excess to overcome the inhibitions to edge and/or corner growth, since the edges and corners have higher curvature than the flat faces of the crystal. The presence of water cloud will further affect the type and rate of growth, but the effect increases with crystal size and will thus not modify the crystal type in its initial stage of growth.

Analyses of radar photographs taken during snow storms reveal that, in general, crystal formation amd most of the subsequent growth occurs near the frontal surface. Presumably then, the situation within the mixing zone associated with the frontal surface is very favourable for rapid snow crystal growth. The vapour density must be at equilibrium with water (in itself a good deal better than ice equilibrium) and water cloud and/or true supersaturation relative to water must exist.

Radar also reveals that the vertical velocity of the snow particles, when the snow is being formed in compact generating elements near the frontal surface, is constant throughout its fall. A study of the terminal velocity of snowflakes, measured from motion pictures at ground level, indicates that the "radar velocities" correspond to velocities of snow aggregates. It must thus be presumed that aggregation occurs within the generating elements at temperatures considerably below the freezing point, and that no growth or major change in the size distributions takes place on the way down. Since the generating zone seems to promote aggregation, the suggestion is therefore that it is a region of turbulence and updraft. This is confirmed by studies of time lapse movies of radar pictures which show that the generating elements are in a continuous state of internal motion.

In summary then, by combining

(a) a new analysis of Nakaya's laboratory experiments

(b) a theory of snow crystal formation

(c) terminal velocity of snowflakes as a function of size

(d) radar observations of the growth and descent of snow,

it has been possible to reach some understanding of the formation, the growth and the subsequent fall of snow.

The present picture is, however, by no means complete. For example, there are still several intriguing problems remaining to be solved in snow crystal studies. Other evidence should be sought for the assumption that the equilibrium vapour density over an ice surface is related to its curvature. We have been able to explain crystal growth in the laboratory at normal atmospheric pressure. The extrapolation of these results to lower pressures has led to a pressure index occurring in the definition of potential temperature and has not been physically justified. There is a need for experimentation at pressures below 1 atmosphere. Intensive investigation on the effects of ventilation on the process of snow crystal formation is also required. There is also the question, which follows from our results, as to why most snowfalls originate near the frontal surface. Is it that the mixing of two air masses of different temperatures produces a region (the mixing zone) having high liquid water content and supersaturation? How does this effect compare to frontal lifting? These are but a few of the problems left for future study.